12-2008

The Application of Electrical Resistivity and Microgravity to Locate Tunnels along the U.S.-Mexico Border at Calexico

Gina Lee Cesin
Western Kentucky University

THE APPLICATION OF ELECTRICAL RESISTIVITY AND MICROGRAVITY TO LOCATE TUNNELS ALONG THE U.S.-MEXICO BORDER AT CALEXICO

A Thesis
Presented to
The Faculty of the Department of Geography and Geology
Western Kentucky University
Bowling Green, Kentucky

In Partial Fulfillment
Of the Requirements for the Degree
Master of Geoscience

By
Gina Lee Cesin
December 2008

THE APPLICATION OF ELECTRICAL RESISTIVITY AND MICROGRAVITY TO LOCATE TUNNELS ALONG THE U.S.-MEXICO BORDER AT CALEXICO

Date Recommended 5-8-08

Director of Thesis - Dr. Andrew H. Wulff

Dr. Michael May

Dr. Stephen Kenworthy

Dr. Rick Toomey

Dean, Graduate Studies and Research Date

ACKNOWLEDGEMENTS

A special appreciation is retained for my advisor, Dr. Nicholas Crawford, director of the Center for Cave and Karst Studies, for his guidance and support in accomplishing this thesis. In addition, I would also like to thank the members on my committee Dr. Andrew Wulff, Dr. Stephen Kenworthy, and Dr. Rick Toomey for their guidance, enthusiasm, and encouragement. Funding for this research was provided by the Department of Engineering's robot grant, Western Kentucky University's Graduate Studies and Research, LANL grant, the Graduate Geoscience Society (GGS), and of course my own personal funds.

Support within Kentucky was provided by Western Kentucky University's Department of Geography and Geology (Mr. Kevin Cary), the Center for Cave and Karst Studies (CCKS – Ms. Leigh Ann Croft and field crew), Department of Engineering (Dr. Stacy Wilson, Michael Howard, Thomas, Rippey, and Steven Miller), Ogden College of Science and Engineering Applied Research and Technology Program (ARTP), the City of Bowling Green's Planning and Zoning Department (Mr. Kyle Bearden), and a business that wishes to remain unanimous that allowed me to conduct research on their property.

Initially, this research was meant to be conducted at Nogales, Arizona, but was changed at the last minute to Calexico, California. I would like to thank those in the Nogales vicinity who provided guidance and information for the original study site. Those involved included Norman Meader of the University of Arizona, Arizona Geological Survey (Mr. Tom McGarvin), the City of Nogales Planning and Zoning Department (Ms. Carmen Zojas), U.S. Customs and Border Patrol (CBP) – Tucson field

office (Agent Lisa Reed and Agent Jose Garza), and U.S. Joint Task Force North (JTFN – participant left unanimous).

Support within California was provided by U.S. Northern Command: Interagency and Coordination Directorate, U.S. Department of Homeland Security (DHS), and U.S. Immigration and Customs Enforcement (ICE) Narcotics and Investigation Group Calexico ASAC office. I would like to specifically thank Agents Ralph Kastner, Robert Kurtz, Matthew Kelly, and Brian McPherson for providing the field crew with security on the border. In addition, I would like to thank Matt Coffelt and Nathan Rinehart for driving out to Calexico and Annie Croft, Michael Howard and Thomas Rippey for flying out to the region to help conduct the study. Additional support in California was provided by the City of Calexico's Planning and Zoning Department, State of California's Department of Conservation Division of Mines and Geology (Mr. Dale Stickney), and the California Geological Survey Library.

Since the Department of Geography and Geology at Western Kentucky University does not have a geophysical component to it, outside assistance was required to understand the theory of the geophysical techniques implemented in the study. This much needed support was provided by attending the Summer of Applied Geophysical Experience (SAGE) program in 2005, which is sponsored by Los Alamos National Laboratory (LANL) branch of the Institute of Geophysics and Planetary Physics, University of California. I would like to thank the faculty of SAGE which included Dr. Scott Baldridge from LANL, Dr. Shawn Biehler from the University of California at Riverside, Dr. Lawrence Braile from Purdue University, Dr. John Ferguson from the University of Texas at Dallas, Mr. Bernard Gilpin from Golden West Coast College, Dr.

George Jiracek of San Diego State University, and Dr. Louise Pellerin from Green Engineering Inc. Additional support was provided by Dr. Aviva Sussman from LANL and Dr. Darcy McPhee from the U.S. Geological Survey. My participation at SAGE led to additional support from LANL. While in attendance my mentors at the lab, whom I could not have completed this thesis, were Dr. Wendee Brunish and Dr. Allen Cogbill.

I would like to again thank all whom gave me support and encouragement in the compilation and completion of this thesis. It is also my hope that the research of this thesis will help support the implementation of a geophysical component to the Department of Geography and Geology at Western Kentucky University.

TABLE OF CONTENTS

PAGE

APPENDICES

LIST OF EQUATIONS

PAGE

Equation:

LIST OF FIGURES

PAGE

Figure:

LIST OF TABLES

PAGE

Table:

THE APPLICATION OF ELECTRICAL RESISTIVITY AND MICROGRAVITY TO LOCATE TUNNELS ALONG THE U.S.-MEXICO BORDER AT CALEXICO

Gina Lee Cesin December 2008 90

Directed by: Nicholas Crawford and Andrew Wulff

Department of Geography and Geology Western Kentucky University

The increasing threat to the United States from terrorist groups and organizations has brought, much needed, attention to the vast U.S.-Mexico border. The daunting task of securing this line of defense has increased at and above the surface forcing smugglers into the subsurface. It is then necessary for geophysical techniques (such as electrical resistivity and microgravity) to be proven or disproven to locate clandestine tunnels along the U.S.-Mexico border. The certainty of success of these techniques is from the success the Center for Cave and Karst Studies at Western Kentucky University has had in Kentucky locating subsurface anomalies later confirmed to be caves. These techniques have been applied at Calexico, within Southern California's Imperial Valley. This region contains clayey lacustrine sediments with a high water table. In addition, the site of observation was located in close proximity to high traffic volume from Mexicali. The combination of these conditions, which are not representative of the entire U.S.-Mexico border, did not allow for an accurate representation of these techniques capabilities. One of the three known tunnels was identified, including additional subsurface features that need drill confirmation. In addition, a low density feature with a 17μgal difference to the surrounding subsurface and high resistive anomaly was observed, which indicates a possible tunnel that had not previously been identified by officials. In conclusion, the combination of electrical resistivity and micro-gravity had possibly identified a clandestine tunnel along the U.S.-Mexico border at Calexico.

CHAPTER I

INTRODUCTION

The U.S.-Mexico border is vast at nearly 2,000 miles in length (International Boundary Water Commission [IBWC], 2008) and is inherently a logistical nightmare in preventing illegal crossings. The focus of this thesis is the application of two geophysical techniques (electrical resistivity and micro-gravity) to non-invasively identify clandestine tunnels along the Calexico, California border.

One of the major vulnerability issues regarding such a vast border is the lack of personnel to monitor that frontier. Through the Department of Homeland Security (DHS) both Customs and Border Protection (CBP) and Immigration and Customs Enforcement (ICE) are tasked with assuring the security of our borders. More specifically, "CBP focuses on security at and between the ports of entry along the border, and is responsible for enforcing customs and immigration laws, with emphasis on the movement of goods and people" (United States-Department of Homeland Security [DHS], 2004; 26). ICE then focuses on the actual enforcement of immigration and customs laws. In order for CBP and ICE to maintain their missions "...inspectors and agents place heavy reliance on various information systems and high technology equipment to secure the borders against terrorists, weapons of mass destruction, illicit narcotics, and other illegal activity" (DHS, 2004; 26). According to a phone interview with Agent Todd Frasier, the improved security at and above the surface of the border has forced smugglers below the surface. Beginning with the implementation of Operation Gatekeeper in 1994, the border has received an increase in personnel, technology, and infrastructure (meaning all weather

roads, stadium lighting, fences, and vehicle barriers). Sections of the border have set a layered defense of a primary fence, all weather road including stadium lighting, secondary fence, and improved technology such as sensors, infrared scopes, and ariel assets. Through the implementation of these land and air defenses along the border, traditional smuggling routes (above the surface) have been disrupted to such an extent that smugglers are forced to go below the surface. According to Agent Frasier these actions indicate that the approach DHS has taken is working.

Approximately 30 tunnels have been found on the Mexican border, and not one was discovered through a geophysical technique. These discovered tunnels have ranged from crude and shallow tunnels, which are quite common, average a depth of 5-10ft and a dimension of 3 x 3 ft. One of the more extravagant tunnels not only included a lighting system, but an elevator. These extravagant tunnels indicate the lengths smugglers are willing to go to in order to get their cargo through undetected. It is important to not only understand the delicacies of identifying these clandestine tunnels, but to identify them expeditiously.

Kentucky's terrain of karst features has encouraged the development and usage of the CG-3M autograv gravity and swift-sting electrical resistivity meters. These meters (specifically gravity) were originally developed for oil companies to find petroleum below the surface. Dr. Nicholas Crawford, Director of the Center for Cave and Karst Studies (CCKS) at Western Kentucky University, had recognized the potential for these meters in the karst region. Before the gravity and electrical resistivity meters, the CCKS had to drill bore holes to locate subsurface features, such as bedrock caves and regolith (unconsolidated material above bedrock) voids. This process was expensive and did not

guarantee finding the subsurface feature. By applying these geophysical techniques to Kentucky and the surrounding regions the CCKS can economize by only drilling where subsurface features have been detected. These subsurface features are indicated by low micro-gravity and high electrical resistivity anomalies.

Building upon the success the CCKS has had in Kentucky in finding caves with these geophysical techniques this thesis proposes to investigate the use of electrical resistivity and microgravity geophysical methods to detect officially known, illegally constructed, tunnels in Calexico, California. The Advanced Geosciences, Inc. electrical resistivity meter and Scintrex micro-gravity meter will be used to test the following hypotheses:

1. Electrical resistivity can be used to detect clandestine tunnels.
2. Microgravity can be used to detect clandestine tunnels.
3. Electrical resistivity and microgravity data can be used in collaboration to support the detection of subsurface voids.

There are varying reasons why non-U.S. citizens in Mexico desire to cross the northern border illegally. These reasons range from seeking a better life/means of providing for ones family to the causation of harm to the U.S. and its citizens. This research was initiated for the prevention of the later.

CHAPTER II

ELECTRICAL RESISTIVITY

Electrical resistivity prospecting is an active, non-invasive, geophysical method that observes the potential differences in the subsurface. In order to correctly evaluate and interpret resistive subsurface features it's necessary to understand the method, conduct accurate observations, and conduct a thorough analysis. This method uses a simple concept that can be widely used. While resistive or conductive subsurface features can be measured it is important to be aware and avoid laying the survey line along cultural features that can pull the current being emitted into the ground. By avoiding cultural interference when obtaining resistive measurements the analysis of the data would produce a more accurate display of the surveyed subsurface for a better interpretation of the area.

Method

Purpose and Application

The electrical resistivity method estimates the conductivity (or, inversely, the resistivity) of a material. Within a geophysical context this method observes the material in a subsurface medium. This approach is commonly used to infer faults, dikes, and horizontal and vertical interfaces between beds (Telford et al., 1990). In addition, this "...technique is one of several electrical prospecting methods for mapping the geoelectric structure of the earth's subsurface" (Lowry and Shive, 1990; 515).

Concept

Essentially the electrical resistivity method measures potential differences to infer a subsurface conductivity distribution. The method is to introduce a dc current into the ground, using both electrodes and a current source, to measure the potential difference (voltage) at points along the surface. Electrical current follows Ohm's law where the current (I) is equal to the voltage (V) divided by resistance (R), see Equation 1.

$$I = \frac{V}{R}$$

Equation 1 - Ohm's Law

Resistance, the opposition to current flow, is dependent on the resistivity of the subsurface media. Resistivity, within a subsurface medium, is a property of the material. It is affect by porosity, water content, salinity of water content, and presence of metal and non-metal materials (discussed further later in the chapter). The resistivity of the medium, Equation 2, cannot simply be calculated by measuring the potential voltage difference per current flow.

$$\rho = \frac{\Delta V}{I}$$

Equation 2 - Resistivity

Due to the various electrode configurations available an apparent resistivity must be computed, see Equation 3.

$$\rho_a = k\frac{\Delta V}{I}$$

Equation 3 - Apparent Resistivity

Apparent resistivity is calculated by multiplying some constant, array used to collect the data, by the potential voltage difference per current flow.

Arrays

There are a number of arrays in use today. Each array has an advantage and disadvantage whether it is applying it in the field or obtaining subsurface observations, see Appendix C for the lateral resolutions on the common arrays. The more common arrays in practice are Wenner, Schlumberger, pole-dipole, and double-dipole. The Wenner array uses equally-spaced current and potential electrodes, and measures the potential voltage difference between the current electrodes, see Figure 3. The Schlumberger array is similar to the Wenner array in that the spread measures the potential voltage difference between the current electrodes, but does not have an isometric electrode spacing, also see Figure 1.

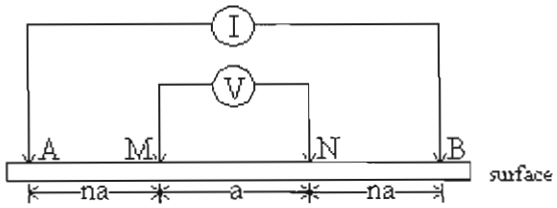

Wenner, $n = 1$ $\quad \rho_a = 2\pi a \frac{V}{I}$

Schlumberger, $n > 2$ $\quad \rho_a = n(n+1)\pi a \frac{V}{I}$

Figure 1 - Wenner and Schlumberger Spread
Source: Telford et al. (1990)

The current electrodes in this array are spaced further from the potential electrodes, compared to Wenner; however, the set spacing between the electrodes remains constant. Increased spacing between the current and potential electrodes provides a better lateral resolution than Wenner, but not as great a depth. In a pole-dipole array a mono-polar current source is observed as the second current electrode is placed at distance infinity, see Figure 2.

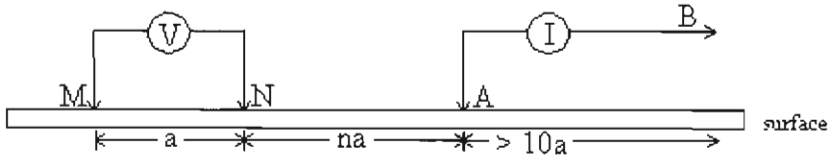

Pole - Dipole $\rho_a = 2n\,(n+1)\pi a \frac{V}{I}$

Figure 2 - Pole-Dipole Spread
Source: Telford et al. (1990)

As the potential electrodes continue to observe the subsurface with increase distance an improved lateral resolution of the subsurface occurs. While this technique provides a sufficient lateral resolution for this study it is not practical. The field in which this study was conducted does not provide sufficient space for the second current electrode at infinity. In a double-dipole array the spacing between the current electrodes is equal to the spacing between the potential electrodes, see Figure 3.

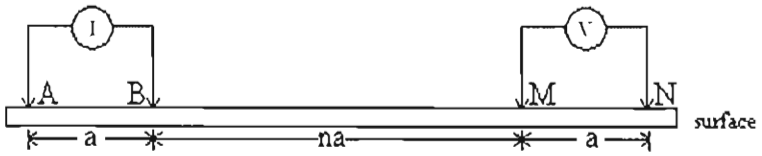

Double - Dipole $\rho_a = n\,(n+1)(n+2)\pi a \frac{V}{I}$

Figure 3 - Double-Dipole Spread
Source: Telford et al. (1990)

Initially in a double-dipole survey current and potential electrodes are in close proximity to one another. As observations continue the potential electrodes increase in distance from the current electrodes. This approach to resistivity observations does not provide the greatest depth of the electrical spreads, but does provide the best lateral resolution given the field constraints.

Measurements

Instrument Used

The resistivity meter used in this study was Advanced Geosciences swift-sting R1. This meter implements any of the common arrays mentioned earlier. In addition, the equipment required to conduct a survey includes the meter itself, switch box, 12V battery, electrode cables, metal stakes, and relevant connectors. During a survey, a single channel is used to acquire the measured potential voltage difference. The swift-sting rate at which work is performed is 200W, while the output current is measured at a continuous 1mA to 2A and an output voltage of 800V. However, the actual electrode voltage is dependent on the current being transmitted and ground resistivity. The observed measurement range of the meter is ± 10V. The input impedance in which the meter is capable of handling is greater than twenty mega ohms. Signal processing of the meter is conducted by continuously averaging roughly six cycles. While the signal is averaged the noise errors are also calculated and displayed as a percentage of the reading. The readings are then displayed as both resistance and apparent resistivity. AGI's meter is capable of suppressing noise better than 100 dB at frequencies greater than 20 Hz and better than 120 dB at power line frequencies (Advanced Geosciences, Inc [AGI], 2006).

Dependence on Subsurface Conditions

The level of resistance a subsurface feature has is dependent on the characteristics of the feature and condition it is found in. Such affecting characteristics of a feature and subsurface condition include porosity of the material, water within pores, salinity of the water, and mineral content of the material. Rock and sediment saturated in electrolyte, mixed solution of salt and water, are less resistive compared to unsaturated material or

fresh water saturation of the same characteristics (Jakosky and Hopper, 1937). The different levels of conductivity found in rocks and minerals make it possible to effectively observe the resistivity of rocks and sediments (see Appendix D). The resistivity ranges located in Appendix D were calculated in a laboratory setting. It is also important to note that there is a large variance in the electrical properties of rocks, due to the fact that small quantities of certain constituents, such as clay, can dramatically change the overall electrical properties.

Analysis

Software Used

The software used to download, evaluate, and model the observed data was M.H. Loke's RES2DINV and AGI's EarthImager. Additional software programs included AGI's Command Creator 1.21 and AGI Administrator. The RES2DINV program, created by both M.H. Loke and Geoelectric Imaging, is a modeling program that enables the user to analyze all the collected data points. The program discards any unacceptable measurement, identified by conducting a positive spatial correlation analysis, before conducting a data inversion. The Command Creator 1.21 two-dimensional program enables the user to program specific programs with set parameters back into the Swift-Sting before going out into the field. The final computer program, AGI Administrator, provides a variety of capabilities that include

- Downloading
- Uploading
- Conversion from one data to another
- Format to another (necessary for analysis and interpretation)

- Calibration
- Three-dimensional and cross-hole command program development.

The RES2DINV program provides a cross-section of the survey's current flow for the particular data set. By initially analyzing the data set with this program the interpreter can determine if the data can still be used or has an unacceptable amount of poor data points, and must be resurveyed. In addition, while observing this portion of the data analysis it is essential to consult field notes when justifying the data's quality. Once the data's quality has been established and merits continued analysis it is modeled using AGI's EarthImager 2D. This program is similar to Loke's RES2DINV program, but has better presentation format.

Processing Data

These software programs determine a two-dimensional model of the apparent resistivity within the subsurface. Within the model of the program there are set rectangular blocks roughly associated with the observed data, which are assigned as datum points. These rectangular blocks are automatically generated by the program and are consistent with the number of datum points. Rectangular blocks are generated to an extent that is equivalent to the depth of investigation. Initially, observation of the datum points should be conducted to remove any obviously bad data, created by either culture or natural events (Loke, 1998). Once the datum points have been corrected (if needed) for points that would skew the results the apparent resistivity is calculated to predict "...the electric potential for a given distribution of resistivity current sources" (Sheriff, 2002; 147), see Figure 4.

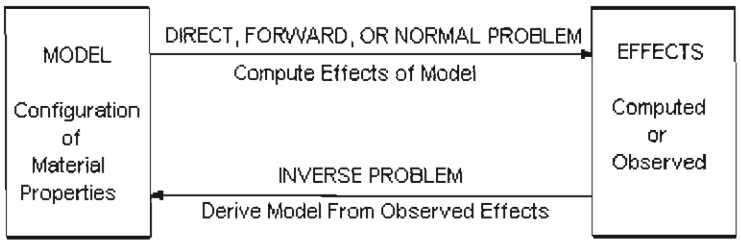

Figure 4 - Forward Modeling Diagram

This process is known as forward modeling and can be calculated by either the finite-difference or finite-element method. The finite-difference method takes the difference between two discrete points of a function to approximate the rate of change, derivative, of that function, see Equation 4.

$$U(x + h) = u(x) + h(3u(x) + 2)$$

Equation 4 - Finite-Difference

The finite-element method is then an approximation to the functions solution. The finite-difference method is faster than the finite-element method when topography does not need to be taken into consideration. After the apparent resistivity has been calculated a subsurface model is constructed that is conforming to the data. This inversion process uses a smoothness-constrained least-squares method that is applicable for different types of data, see Equation 5.

$$(J^T J + \mu F)d = J^T g$$

where $F = f_x f_x^T + f_z f_z^T$, f_x = horizontal flatness filter,
f_z = vertical flatness filter, J = matrix of partial derivatives,
μ = damping factor, d = model perturbation vector, and
g = discrepancy vector. (Loke, 1998)

Equation 5 - Jacobian Matrix

There are two least-squares optimization techniques, Gauss-Newton and quasi-Newton, that are used to calculate the Jacobian matrix. Ultimately, there are three options to calculate the matrix, which is to use either method or a combination of both. These

methods are iterative conducting algorithmic calculations to best fit calculated values with measured values, while the optimization function attempts to reduce the difference between them. The overall difference between the calculated and measured values is the root-mean-square (RMS) error. There are hazards in the analysis process of resistivity data that include data evaluation, depth determination, and ground conditions. It is necessary to evaluate and remove any bad datum points, because useless data into the equation produces a useless solution. Moreover, it is important to keep in mind that the rectangular blocks have an exponential decrease of resolving power with depth. In addition, ground conditions have a great influence as to whether the resistivity meter can even be used. If the top ground layer is to dry electrical current will not flow through the layer. Likewise, if the top layer is too conductive the voltage difference at the potential electrodes may be too small to measure (Loke, 1998).

Data Display

The data is graphically displayed into three pseudo-sections, in consecutive order from top to bottom. The first pseudo-section represents the measured apparent resistivity. Secondly, the calculated apparent resistivity is represented. Lastly, the third pseudo-section is the inverse model of the data that best represents the survey's subsurface. Within these pseudo-sections the distance measured is placed on the x-axis, while the approximate depth of evaluation is represented on the y-axis. The inversion model of the data is displayed with the iteration, RMS error percent and normalization values. In addition, a color scheme representing resistivity ranges are generated for each pseudo-section.

CHAPTER III

GRAVITY

Gravity prospecting is a passive, non-invasive, geophysical method used to infer density variations in the subsurface. In order to obtain the depth and diameter of subsurface features it is important to understand the method being used, obtain precise measurements, and conduct a thorough analysis. Understanding the method behind gravity prospect is simple, but can have a wide range of applications. While the application of this technique may be wide ranging the measurement process must be consistent in order to avoid obtaining skewed data. In addition, by being consistent in obtaining measurements the interpretation process of the analysis section becomes simple, and ultimately conclusive.

Method

Purpose and Application of Gravity Measurements

The gravity method derives the subsurface distribution of density to determine information about subsurface features. More generally, Picha (1973) states that gravity prospecting is a subset of geophysics, which "...deals with and investigates physical phenomena and properties of the whole earth or of its more extensive regions" (pp. 15). This method has been used for geophysical research, environmental monitoring, and exploration and resource management; however, geophysical research is the most extensively used. Examples of the research that have been conducted include detection

of vertical crustal motion, volcanic magma flow, postglacial rebound studies, earthquake research, and long period tidal monitoring (Micro-g LaCaste [Micro-g], 2006).

Concept

Primarily, the gravity instrumentation used in this study measures the electrostatic restoring force placed on a spring to balance the gravitational force. The gravitational force on a proof mass follows Newton's law of gravitation, see Equation 6,

$$F = \gamma\left(\frac{m_1 m_2}{r^2}\right)r1$$

Equation 6 - Newton's Law of Gravitation

where the gravitational force is inversely proportional to their distance. In order to measure for gravity Newton's law of gravitation is algebraically transformed to Equation 7.

$$g = \left(\gamma\frac{M_e}{R_e^2}\right)r1$$

Equation 7 - Measuring Gravity

Where γ is the universal gravitational constant, M_e is the mass of the earth, R_e is the radius of the earth, and r_1 is the extension downward toward the center of the earth (Telford et al., 1990; 7). The gravity field varies over the surface of the Earth through the affects caused by elevation, latitude, earth tides, terrain, and subsurface density variations. Since the Earth is very nearly a spheroid, with a bulge at the equator and a flattening at the poles, gravitational attraction varies with the inverse square of the distance between the center of the Earth and the location of observation, known as the free-air effect. The additional mass in an increase of elevation applies a positive

gravitational attraction opposite to that of the free-air effect. Based on "...the gravitation attraction of a horizontal slab, of infinite extent and of thickness equal to the elevation difference," (Seigel, 1995; 5) the Bouguer gravity effect is calculated. Both the free-air and Bouguer effect can be combined to calculate the elevation effect. Just as elevation affects gravity, so does the terrain within the region of investigation. The excess mass of a mountain, just as a deficiency of a valley, causes the spring within the gravimeter to pull towards or away from the affecting feature. In addition, gravitation acceleration changes with time. This effect on gravity is caused by Earth-tides, atmospheric pressure, precipitation, and sea level changes. Earth's tides, caused by the gravitational attraction of the moon and sun affects gravity by pulling more of the Earth's mass towards the direction of the gravitational attraction. Changes in atmospheric pressure such as an increase in pressure causes a decrease in observed gravity. As the mass of an air column over the observed point the proof mass gravitates slightly away from the center of the Earth, causing a decrease in observed gravity. Precipitation is another factor that can affect gravity measurements. Rainfall causes an increase in moisture content and groundwater level that fill porous soils and rocks, including lakes and rivers (Seigel, 1995). Sea-level changes can also affect gravity readings if the line of observation is close to the coast. Ultimately, these factors that cause variations in the gravitational field can be calculated and accounted for. The remaining affect on gravity is subsurface density variations. A subsurface area of lower density produces a low gravity anomaly. The greater the difference in density within the observed traverse the more pronounced the feature.

Dependence on Subsurface Densities

According to Grant and West (1965) "[d]ensity is a physical property that changes significantly from one rock type to another..." (pp. 189). It is important to note that rocks closest to the point of observation have greater influence on the measured gravity. Sedimentary, igneous, and metamorphic rocks have varying densities based on several factors. These factors include porosity, composition, compaction, texture, and mineralization. This study does not require the discussion of all these factors, but its important to have mentioned them.

Sedimentary rocks are "...formed from sediment that has accumulated in layers, or a chemical rock formed by precipitation from solution, or an organic rock consisting of the remains of the secretions of plants or animals" (Sheriff, 2002; 309). According to Grant and West (1965), there are four major groupings that sedimentary rocks fall under. They are, in order of increasing density: soils and alluvia, sandstones and conglomerates, shales and clays, and calcareous rock including limestones and dolomites (pp. 192). Density levels of sedimentary rocks are dependent on an assortment of factors. Both dry/wet bulk density and the age/depth of burial increase or decrease the density level of sedimentary rocks.

Grant and West (1965) states that "...[d]ry bulk density refers to macroscopic specimens in a completely desiccated state, whereas wet bulk density implies that the specimen is fully impregnated with water" (pp. 192). The porosity of the sediment is of great importance when evaluating the level of importance with bulk density, wet or dry. The development of wet or dry bulk density is also caused by the level of the water table,

which in turn is typically dependent on the climatic region being arid or moist. In regards to the porosity "[s]ediments that remain buried for long periods usually consolidate and lithify, resulting in a reduction in porosity and an increase in density" (pp. 192).

Igneous rocks are less porous and as the silica content falls the density rises. Even though igneous rocks are more dense than sedimentary rocks there is considerable overlap. "Density usually increases with the degree of metamorphism because the process tends to fill pore space and recrystallize the rock in a denser form" (Telford et al., 1990; 18). Hence, rocks with greater degrees of metamorphism tend to be more dense, producing positive gravity anomalies, see Appendix E for rock densities. When evaluating the density of any rock it is important to, according to Garland (1965), evaluate "...the minerals of which it is composed, and partly on the proportion of its volume which is occupied by pores" (pp. 101). Remember, if the rock is porous, water saturation (bulk density) must be taken into consideration.

Approach

Earth's gravitational acceleration can be measured by two methods, absolute and relative. The absolute method is the true gravity at the observation point. This method is usually more expensive and time consuming than relative measurements. The relative form of measuring gravity "...reflects the differences in gravitational acceleration...at one station...compared to another" (Lillie, 1999; 234). The absolute method was not used in this study, and will therefore no longer be discussed.

Measurement

Instrument Used

There are about two to three gravimeters out in today's age. Relative gravimeters are compact and designed to handle reasonable environmental conditions. The gravimeter used in this study was Scintrex's CG-3M autograv. Based off the Worden system, the CG-3M was developed to be easily manufactured, have mechanical simplification over older models, tolerate rough field use, have temperature stabilization, obtain a resolution of 1 μGal, read with a standard deviation of 5 μGal or better, and have electronic and software control of the measurements. The system works using a fused quartz spring and produces an electrostatic restoring force to balance the proof mass back to the null position, originally displaced by the gravitational force. A capacitative displacement transducer senses the position of the proof mass. A dc voltage, controlled by an automatic feedback circuit, is applied to capacitator plates to produce an electrostatic force on the proof mass to bring it back to its null position. The feedback voltage is converted to a digital signal and transmitted into storage in the solid state memory (Seigel).

Corrections for Observed Gravity Values

Earth-tide affects on the gravitational field are caused by the sun and moon and can contribute up to a difference of 0.3 mGal per hour. This correction becomes significant in micro-gravity surveys. Instrumental drift can develop over a short and long period of time. In a short term drift accuracy restoration of the readings is done by

establishing a base station as a reference density location. Initially within a survey two base station readings are collected before the observation of a survey line begins. After an arbitrary period of time passes and a short term drift occurs the gravimeter is taken back to the base station for two or more gravity readings. The difference of the readings during that period of time can then be calculated to ultimately correct the gravity readings for the springs drift. Over long periods of time the spring experiences drift, and as such readings that were observed months ago at a particular location and time are no longer the same if observed at present. In order to resolve this issue repeat measurements at an accommodating station can be made over a period of at least 48 hours. Gravity values with time are calculated to determine the residual long term drift rate, to then adjust this factor. Additionally, atmospheric pressure changes can affect the gravitational field. Seigel states that "...on normal weather days will only affect micro-gravimetric surveys (only in a minor way), there may be atmospheric conditions which can cause significant effects at the μGal level" (pp. 40). There are two ways in which this correction can be made. The first is to read a barometer with a resolution of 0.1 kPa at every station or to have to barometer kept stationary, for surveying in small areas, and read periodically. The second is to periodically measure back to a gravity base station "...to correct for the pressure-induced effect through the linear drift correction" (pp. 41); however, for normal days start, mid-day, and end of day measurements back at the base station is sufficient. Changes within the groundwater and surface water levels, caused by precipitation, may affect the observations of Earth's gravitational field. This correction may not be required, depending on the topography a seasonal change. The latitude effect on the gravity field is corrected by established values from a differentiated equation. Correction

for the elevation is conducted by accounting for both the free-air and Bouguer effects. Terrain effects should be corrected for if there is significant terrain changes that would cause the spring within the meter to be influenced. Fortunately, no such correction was needed for this study.

Obtaining High Precision Measurements

The precision of data obtained from observations of a study depend on the care taken during observations. There are two factors (Instrument and External) that need to be considered for precision measurements. The instrument factor encompasses shock and vibration, power-down, extreme temperature shocks, elastic relaxation, leveling, change of battery, calibration, and long and short term drift (previously discussed). Shock and vibration occurs when the instrument is exposed to long periods of sever vibration. For short periods of variations (e.g. driving the instrument to the study site) the instrument is set at the base station for a period of at least thirty minutes to settle the spring for precise measurements. If power-down occurs the instrument experiences a temperature shock that may take at least a day to adjust when powered back up. External extreme temperature shocks occur when transferring the instrument from a relatively cool environment to an extremely warm environment. This instrumental factor can be avoided by keeping the instrument in an environment similar to the outside temperature. Elastic relaxation occurs when the spring inside the meter does not quickly return to its null position. This factor can have an effect less than 10 to 20 μGals, obviously a significant effect for microgravity surveys. Elastic relaxation can easily be accounted for by placing the instrument on a tripod and leveling it anytime it is moved. Leveling is the process by

which "...the measurement system is aligned along the plumbline, i.e. the direction of the gravity vector at the station" (pp. 25). It is important to level the gravimeter as accurately as possible, because "...if $\theta = 10''$ of arc, the error will be 1 μGal, but if $\theta = 20''$ of arc, then the error will increase to 4 μGal" (pp. 25). In the field if the supply battery of the instrument loses its useful charge and requires changing a change in the observed gravity level may occur. Favorably, for the surveys conducted in this study the supply battery never reached the end of its useful charge. Calibration of the instrument must be conducted. Initially when the instrument is constructed from the factor frequent calibration checks should be made during the course of the year. After a period of time in operation these checks can be conducted once a year. Both long and short term drifts have already been discussed and will only be mentioned here. The external factors that affect high precision measurements are seismic noise, selection of station location, wind-induced vibration, station elevation, and atmospheric pressure. Seismic noise can be caused by either man-made or natural sources. Man-made sources include traffic and industrial noise, while natural sources include earthquakes, local earth resonances, and microseisms. Man-made sources of seismic noise are encountered in urbanized areas; however, natural sources of seismic noise can be encountered anywhere. A major earthquake event can make a gravimeter useless for periods as long as several hours. Microseisms, relatively continuous levels of seismic noise such as wave action from shore lines or passage of rapidly moving pressure fronts, vary from time to time. Additional seismic noise sources include wind-induced vibration and tree root movements. Gravimeters such as the CG-3M automatically digitally averages successive measurements. The gravimeter is also capable of rejecting individual measurements

(smart signal processing) that deviate from the mean by more than a designated number of standard deviations of the measurement. The selection of a survey line is highly important for usable gravity readings. Survey lines should be conducted away from areas of high seismic noise sources, un-firm ground, and discernable terrain features. Wind-induced vibrations can also cause difficulty in obtaining usable gravity readings. A solution to wind-induced vibrations is to have the observer position themselves in the path of the wind when making observations. The station elevation factors can cause large errors in gravity readings. Seigel states "...that if the density of the local rock is 2.5g/cm^3 then a one metre elevation error will cause an error in the final gravity data of 0.20 mGals" (pp. 33). Such an error can cause a microgravity survey to be rendered useless. In order to obtain usable microgravity readings it is necessary to establish the relative station elevation with ± 2cm accuracy. Atmospheric pressure is the remaining external factor that must be considered. As discussed previously, the solution to the atmospheric pressure factors is to periodically conduct base station observations through the survey. An extraneous factor for consideration in obtaining high precision measurements is positional accuracy. Although not as critical as elevation accuracy, positional accuracy is still notable. Considering "...the maximum result of an error of ± 5m in the north-south position of a station will give rise to an error of ± 4 μGals at mid-latitudes, and less elsewhere" (pp. 54) the position of the instrument on a survey line is relatively important (Seigel, 1995).

Analysis

Software Used

The software used to download, evaluate, and graph the observed data was Windows XP and Geosoft's Oasis Montaj. Oasis Montaj is both a mapping and processing software; however, within this study the mapping portion of this software was not used. This software has a database capable of storing and evaluating large amounts of data. After the data has been evaluated it is exported into a Windows Microsoft Excel spreadsheet for graphing.

Processing Data

A link between the computer and the gravimeter was established and through that link data were downloaded into a text file. Within this text file an initial evaluation of the data occurs. At this point the observer must remove any bad data points collected to ensure good data quality. Once the data within the text file have been evaluated and approved they are opened in Oasis Montaj. Within the software, corrections on the elements affecting the observed gravity field such as elevation, latitude, earth-tides, and terrain effects (if applicable) are conducted. Completion of the corrections leaves subsurface density variations, known as the Bouguer gravity, as the sole contributor to gravity variations (anomalies). After these readings have been determined the spreadsheet is then saved and imported into Microsoft Excel for display.

Data Display

The data is displayed as a simple double-axis graph. This double-axis graph is generated to display the calculated gravity compared to the elevation changes of the

survey line. The left y-axis displays the Bouguer gravity in μGals, while the top x-axis represents the station number (typically the distance on the survey line). In addition, the right y-axis represents the relative elevation of the survey line. With a simple key denoting the elements within the graph the graphical representation of the subsurface is ready for interpretation.

Depth and Diameter of Features

Calculating a buried object at depth, in this case the simple shape of a sphere, through its gravitational attraction is done by measuring its vertical gravitational component (Δg_z), denoted in Equation 8:

$$\Delta g_z = \frac{4\pi}{3} \frac{R^3 (6.67 \times 10^{-11})(\Delta\rho) z}{(x^2+z^2)^{\frac{3}{2}}}$$

Equation 8 - Vertical Gravitational Component

Where R is the radius of the sphere, $\Delta\rho$ is the density difference between the sphere and surrounding material, x is the horizontal distance of the observation point to the sphere, and z is the vertical distance of the center of the sphere to the surface of the earth.

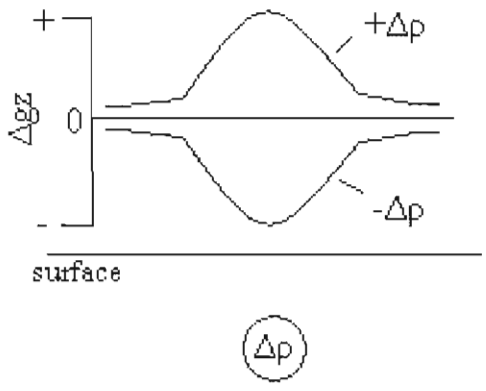

Figure 5 - Proportionality of Mass to Gravity

Source: Lillie (1999)

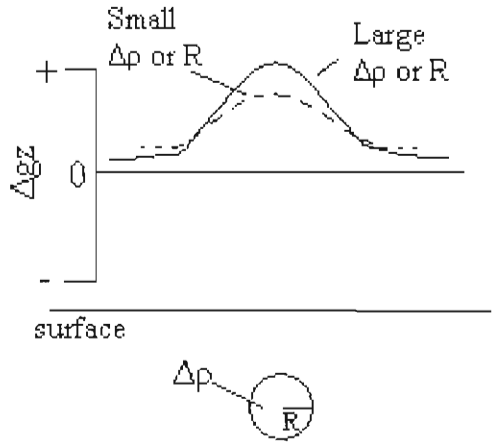

Figure 6 - Proportionality of Sphere to Amplitude
Source: Lillie (1999)

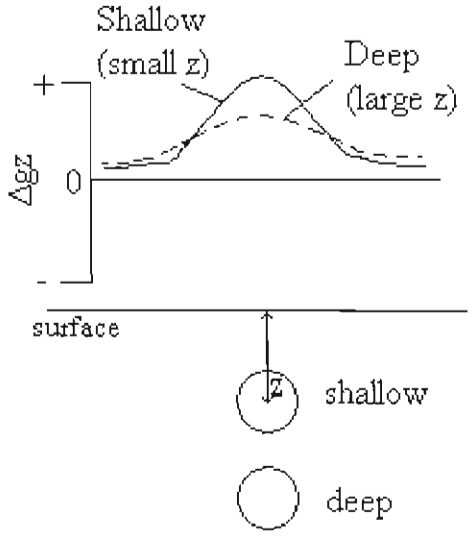

Figure 7 - Reading Depreciates as Depth Increases
and
Figure 8 - Reading Width Increases as Sphere Increases with Depth
Source: Lillie (1999)

An adequate interpretation of a two-dimensional data plot requires the understanding of four fundamental principles:

1. Gravity is proportional to mass so that a mass excess causes an increase in gravity, while a mass deficiency causes a decrease in gravity (Figure 5).
2. The more massive the sphere, either through its $\Delta\rho$ or R, the greater the amplitude (Figure 6).
3. The anomaly amplitude decreases as the sphere's depth increases (Figure 7).
4. The anomaly's width increases as the sphere increases in depth (Figure 8). (Lillie, 1999)

These principles should serve as guidelines to interpreting two-dimensional graphs.

CHAPTER IV

PHYSIOGRAPHY AND GEOLOGY

South-central Kentucky Regional Geology

The state of Kentucky is composed of four structural provinces known as the Illinois and Appalachian basins, Cincinnati arch, and the Mississippi Embayment. South-central Kentucky lies within the Cincinnati arch, which "...extends from the Nashville dome in Central Tennessee through Central Kentucky to Northwestern Ohio..." (McDowell, 1985; H53), see Figure 9.

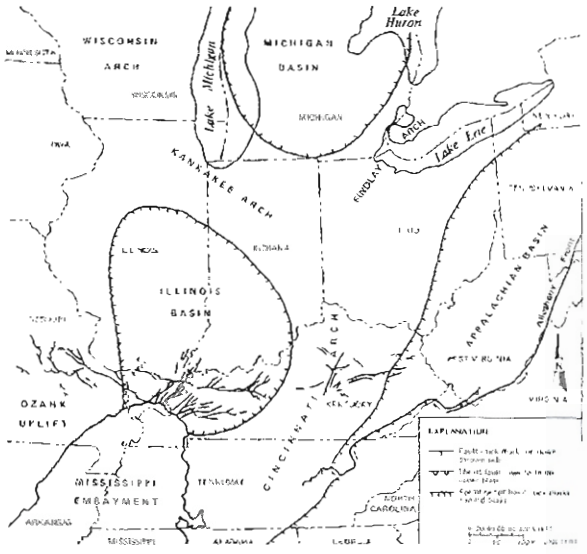

Figure 9 - Kentucky Structural Provinces
Source: McDowell, 1985

Physiographicaly, South-central Kentucky is situated on the Mississippian Plateau, also known as the Pennyroyal, see Figure 10.

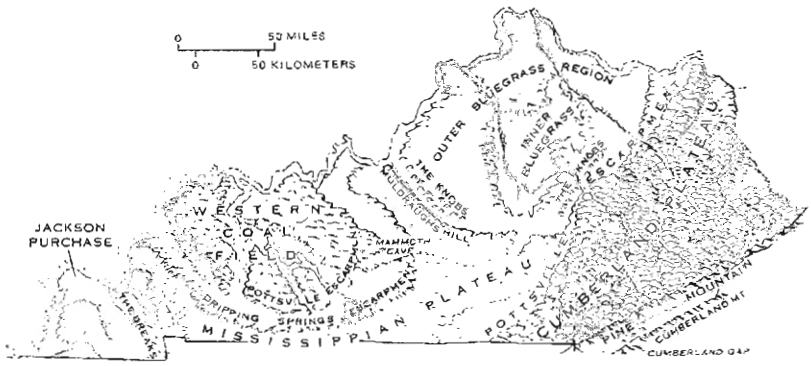

Figure 10 - Kentucky Physiography
Source: McDowell, 1985

East of the Mississippian Plateau is the Cumberland Plateau lined on the west by the Pottsville Escarpment. To the northeast the plateau runs up to the belt of knobs (known simply as The Knobs) and Outer Bluegrass Region, while to the northwest leads into the Western Coal Field lined by both the Pottsville and Dripping Springs Escarpments. On the westernmost boundary of the plateau is the Jackson Purchase lined to the east by the Land between the Lakes, locally known as The Breaks (Newell, 1985).

Mississippian Plateau

Within the upland plain of the Mississippi Plateau is an intricate pattern of sinkholes and caves. Common topological factors of this region are collapsed topography, sinking streams, and extensive cave networks (Newell, 1985). The underground streams, developed by the dissolution of the carbonic rock, provide the communities in these regions with a natural and well-developed drainage system. These landforms are known as karst and are also sensitive to environmental factors. The minimal soil cover in karst regions provides minimal filtering causing poor groundwater. In addition, "[s]inkholes and karstic lakes play the role of 'windows' to underground

aquifers and in the natural drainage network" (Taminskas et al., 2006; 62). Typically sinkholes are dry, but can quickly fill during periods of heavy rainfall.

Karst and the Subsurface

Karst can be found in all kinds of regions and are most frequently located in carbonate terrain. Karst is developed by the dissolution of carbonate rock through acidic rainfall. "The highly varied interactions among chemical, physical, and biological processes have a broad range of geological effects including dissolution, precipitation, and sedimentation and ground subsidence" (pp. 62). A South-central Kentucky stratum is mainly composed of Ste Genevieve and St. Louis Limestone. The St. Louis is overlaid by the Ste. Genevieve Limestone, which is divided into three members: The basal Fredonia Limestone, Rosiclaire Sandstone, and the Levias Finestone. In this region "...the Ste. Genevieve and St. Louis Limestone are thinner and are divided at a zone of a calcarenite-cemented chert 'breccia' (conglomerate)" (Grabowski, 1985; H24). According to Grabowski (1985) the majority of the Mississippian system in Kentucky is assembled of marine sedimentary rocks. Furthermore, "...a widespread shallowing of the seas during Mississippian time, with basinal and prodetaic shales and siltstones succeeded by shelf limestones and dolomites and coastal sandstones and shales" (pp. H19).

Southern California Regional Geology

Imperial Valley, on a grander scale, is found within the Basin and Range Province in Southeastern California. The valley is located within a basin, also known as the Salton

Trough which encompasses two additional valleys (Coachella and Mexicali). This region has been going through rapid geomorphological changes with the majority of its transformation taking place in the Cenozoic Era. The physiological features of this region has also greatly influenced the development of the valley, but none more than human influence, discussed later in the chapter.

Cenozoic Era of the Salton Trough

The Salton Trough is the northern extension to the Gulf of California, and at one time maintained marine organisms. Through unique regional parameters the Salton Trough has undergone major physiological adjustments. Regional parameters include orogeny, uplift (by both orogenic and isostatic processes), and rifting. The trough was gradually bounded by mountain ranges and a dialectic barrier, isolating it from the Gulf of California and masses of air moisture carried by westerly winds. The development of these physiological features combined with natural heat conditions brought forth the existence of the Colorado Desert. Even though physiological features dictated desert conditions, previous marine conditions in league with the Colorado River's influx of overflow and sediment deposit provided the region with some of the most fertile soil in the world, see Appendix A for the regions geologic time scale.

Crustal Deformation

Nearly 30 million years ago the evolvement of, what is now, the modern-day basin begins to appear through east-to-west stretching (Danielson, 2000; 1-2). This pull-apart basin is continually being formed through run-off (from the minimal precipitation in

the region), tectonic uplift, sediment and wind erosion, and the irrigation being conducted.

Gulf of California Extension

Before the region arrived to its modern day state the Salton Trough was nearly all under marine waters (Morrison, 1991; 334). According to Waters (1983) "[t]he Salton Trough is the landward extension of the depression flooded by the Gulf of California..." (pp. 373). Reheis (2005) states that "[t]he marine section was strongly affected by the Colorado River, which rapidly filled the area with fresh water and sediment, reducing the marine influence" (pp. 15). The continued influence of the Colorado River had lead to an initial incursion of a deltaic barrier between the depressed basin and the gulf.

Formation of the Colorado Delta

The mighty Colorado River begins its decent as snowmelt from the Rockie Mountains. Uplift of the lower Colorado River, according to Morrison (1991), between 5.5 and 4.3 Ma initiated the formation of the Colorado delta and by 4 Ma "...spanned the Salton Trough and isolated its northern part from the Gulf of California" (pp. 334-35). Gilmore and Castle (1983) "...suggest that the existing divide between the sub-sea-level Salton basin and the Gulf of California is maintained in part by tectonic uplift" (pp. 474), and not solely on the expansion of the Colorado River delta. Gilmore and Castle go on to suggest "...that continuing crustal swelling along the deltaic crest...has biased the flow of the Colorado River away from the Salton basin...and into the Gulf of California" (pp. 474).

Continued Crustal Deformation

Crustal deformation continues across the region producing a diverse conglomeration of interdependent elements. According to Morrison (1991), these diverse assemblages of interrelated elements include:

> (1) Left-lateral faults, oriented at high angles to the general trend of the dominant right-lateral fault systems...
> (2) Zones of seismic activity, high heat flow, hydrothermal activity, and local volcanism...and
> (3) Low hills of uplifted Pliocene and Pleistocene sediments, deformed by closely spaced, east-west trending transpressive folds, which occur within and adjacent to the major right-lateral fault system..." (pp. 334).

Within this rift, as the lithosphere continues to stretch, magma is brought closer to the surface. By thinning of the lithosphere and mountain building to the west the saline water in the Salton Trough is boiled and evaporated, leaving a great amount of sodium chloride (NaCl) and producing a regional desert. Periodically the course of the Colorado River would divert into the Salton Trough accumulating, according to Morrison (1991), fine-grained deltaic and lacustrine deposits within the south and central parts of the basin (pp. 335).

Lake Cahuilla

"Lake Cahuilla originated by periodic overflow and diversion of the Colorado River into the Salton Basin" (Morton, 1977; 19). Waters states that (1983), Lake Cahuilla formed several times in response to the western diversion of the Colorado River into the Salton Trough (pp. 373-74). Eventually the Colorado River would divert back to

its old course leaving Lake Cahuilla to slowly evaporate. "The rediversion of the Colorado River could have been triggered by tectonic movements, base-level changes, or a large-flood" (pp. 375). Once the lake was evaporated the Colorado Desert would return.

Colorado Desert

The southwest desert, according to Thorne (1986), had developed because the majority of the moisture brought by the prevailing winds off of the Pacific Ocean precipitated on the western slopes of the mountain ranges lining the Salton Trough. "As the air masses descended the transmontane slopes, they heated up adiabatically and became a drying force" (pp. 642). In addition, Marks states (1950), the desert is formed into four physiographic provinces that include (1) valleys of alluvial soil, (2) mesas of mixed alluvial-colluvial soils, (3) mountain pediments of cemented gravelly or coarse sandy soils, and (4) mountains with rough broken lands (pp. 192). The desert was physically determined by two factors: (1) regional mountain building upheaved by block-faulted mountains that run northwest to southwest (pp. 178-9), see Appendix B for the Salton Trough Fault Zones.

Securing the Imperial Valley

The soils of Imperial Valley had drawn the attention of settlers traveling west. Rich in nutrients brought by sediment deposits left by the Colorado River made the valley an attractive prospect for farmers. The only thing that lacked in the valley was an irrigation system that would maintain crops throughout the hot arid climate associated

with this region. A channel was cut between the Colorado River and the Salton basin to provide settlers with the resources they needed to produce their crops. Little did settlers know that a shift in the Colorado Rivers would soon jeopardize their crops. In 1905 the river did just that and settlers were soon in desperate straights. Over eighty-percent of the river was now being poured into the valley. Even though it would take 20 years for the Salton Trough to fill the irrigation company went, immediately, to work on trying to solve the issue. It wasn't until countless defeats of trying to redivert the river that it was finally diverted. It took two years, a number of engineering resolutions, and nearly two million dollars to put the Colorado River back onto its southerly course into the Gulf of California. Even though it seemed as if the Colorado River was under control it wasn't until the completion of the Hoover Dam, in 1935, that the valley was truly safe from being inundated from the river (Schonfeld, 1969).

Calexico

Specifications of the Calexico study area are essential to understand for a correct interpretation of the observed data. Soil classification of this region is Holtville-Imperial. Holtville is defined as clayey over loamy, while Imperial is fine. The silty clay loams of Imperial Valley retain a high water table of a depth greater than six feet. Holtville-Imperial soils average a permeability of 0.06-.2 inches per hour and have a high shrink-swell potential (Zimmerman, 1981).

CHAPTER V

STORM SEWERS

The storm sewers case study observed resistivity and micro-gravity data over three storm sewers of different construction. High-density polyethylene (HDPE), reinforced concrete (RCP), and corrugated metal pipe (CMP) are commonly used materials for storm sewer construction. Objectives for the study included:

- Determining the effective interval spacing for electrical resistivity
- Concluding what a subsurface feature of specific diameter may appear as
- Comparing and contrasting features of commonly used material for storm sewer construction

All observed storm sewers were relatively shallow and a consistent diameter of approximately two to two and a half feet. Also, 21 electrodes were used instead of the typical 28 because there was only one point on the line that needed to be observed.

IP Site

The IP site had the high-density polyethylene (HDPE), polymer, storm sewer. HDPE is a high density plastic. In addition, this site was arbitrarily chosen to determine effective interval spacing required to identify shallow-subsurface voids of two to two and a half feet diameter. The determination of suitable interval spacing at this site was used throughout the project. Five traverses of varying interval spaces were conducted over the storm sewer to determine the most suitable spacing for the project in order to most

effectively observe a known resistive subsurface feature, void within a medium. The layout at the IP site is shown on Figure 11.

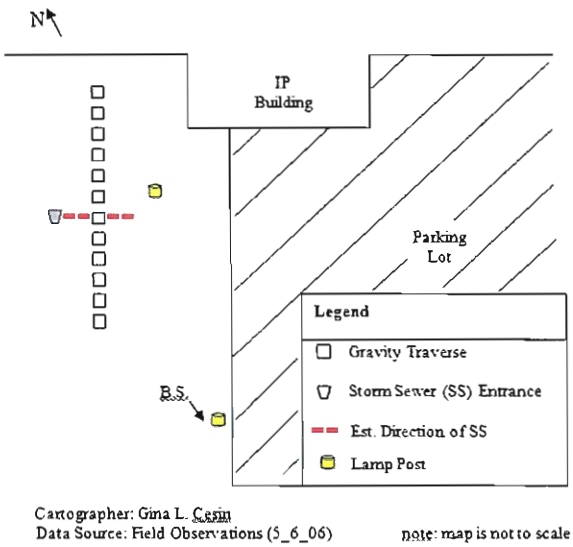

Figure 11 - High-Density Polyethylene Study Site
Source: Field Observations (5_6_06)

The traverse illustrated in Figure 11 represents both the gravity and electrical resistivity lines that were measured. Initially, electrodes were attached to their respective stake at an interval spacing of two. Figure 12 illustrates a representation of the subsurface, with micro-gravity and electrical resistivity.

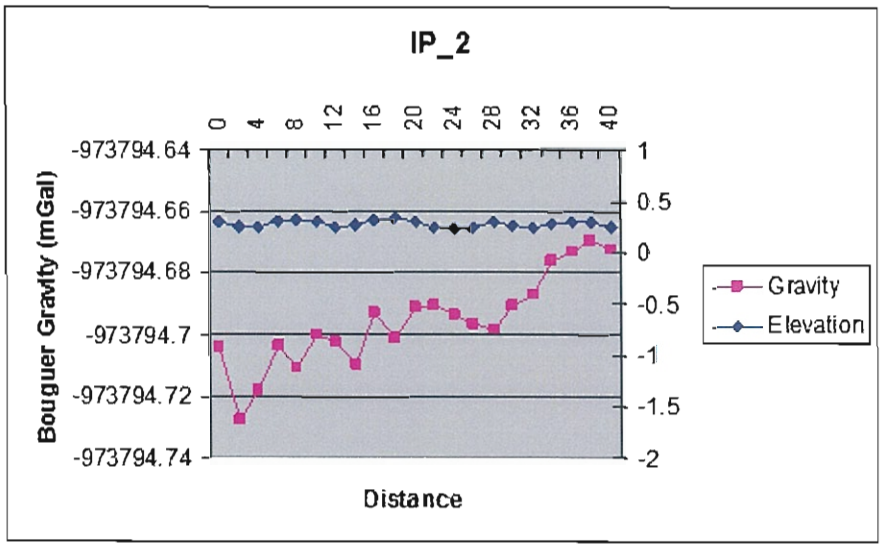

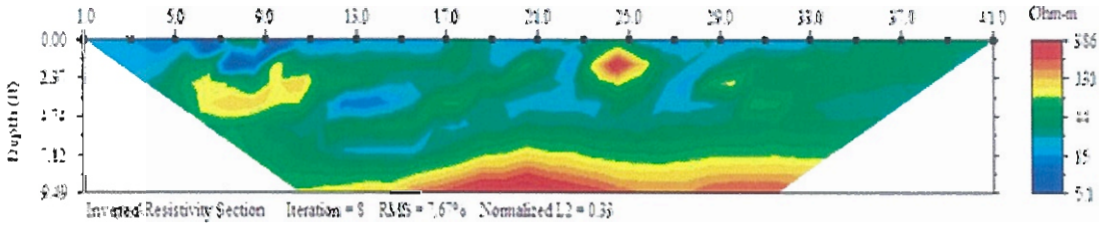

Micro-gravity and Electrical Resistivity: 2 ft spacing

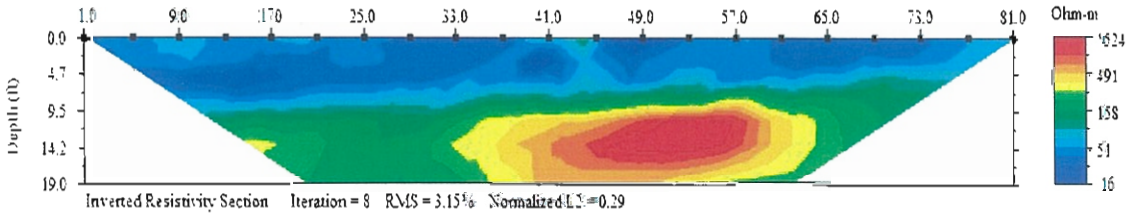

Electrical Resistivity: 4ft spacing

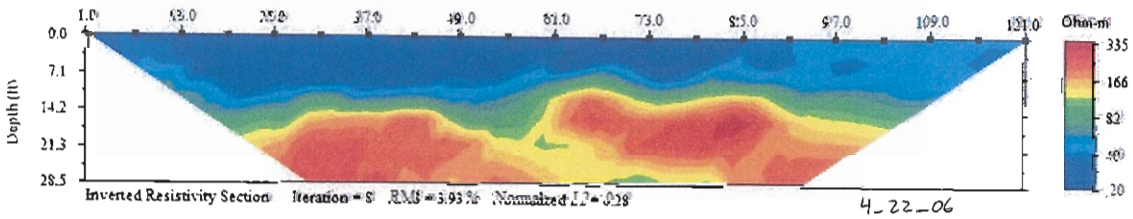

Electrical Resistivity: 6ft spacing

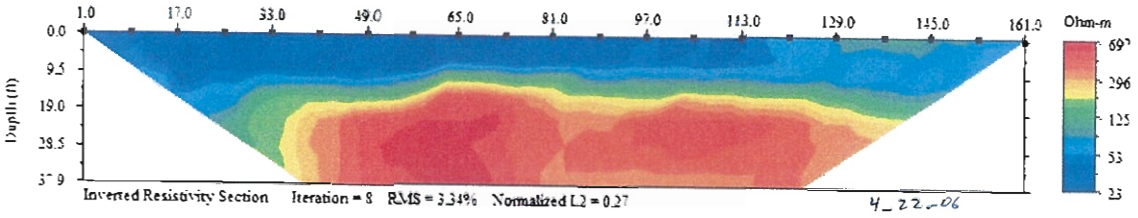

Electrical Resistivity: 8ft spacing

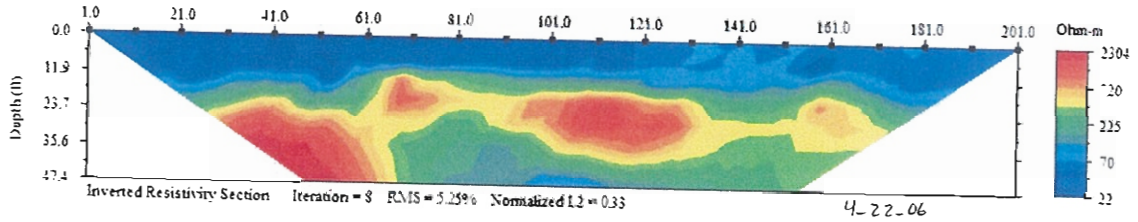

Electrical Resistivity: 10ft spacing

Figure 12 HDPE Micro-Gravity and Electrical Resistivity Data
Source: Field Observations (5_6_06)

Micro-gravity was automatically collected using a two-foot spacing. The gravity meter does not depict anything unusual to the surrounding subsurface, while the resistivity measurement of the subsurface at a two foot interval spacing identifies the feature. When the interval spacing is increased the subsurface feature initially observed on a two-foot spacing becomes diluted. Using a two-foot spacing to identify a subsurface feature of approximately 2 ft diameter is effective for resistivity measurements. The lack of detection from micro-gravity measurements is consistent with the high-density material being observed.

CLP Site

The CLP site had the corrugated metal (CMP) storm sewer. Corrugated metal is folded and/or intertwined metal. This site was heavily over-brushed making it difficult to collect measurements directly over marked points on the traverse; however, the slightly

modified points of measure were not consistent for both micro-gravity and electrical resistivity. The slight modifications for the points of measure were necessary due to the physical characteristics of the sight. Even though the micro-gravity and electrical resistivity traverse line were not in direct line with each other the calculations for the data were still measureable. The layout of the site is shown in Figure 13.

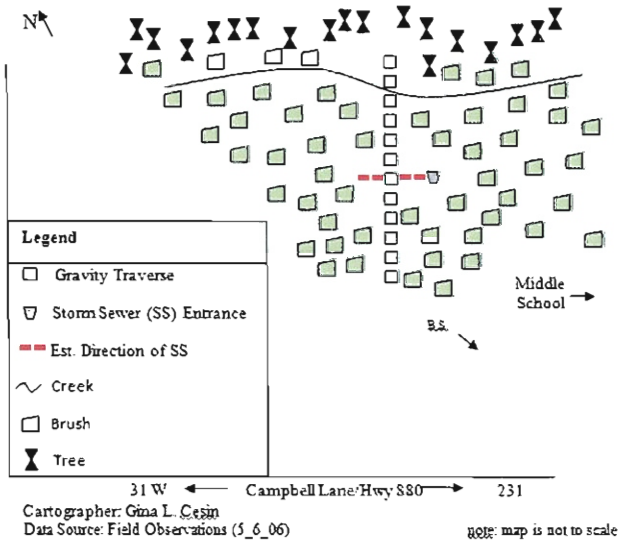

Figure 13 - Corrugated Metal Pipe Study Site
Source: Field Observations (5_5_06)

The traverse illustrated in Figure 13 does not specifically denote two separate lines of measurement for the gravity and electrical resistivity measurement, because the differences of measurement location was to insignificant to be displayed on field observation notes. Even though measurement locations were too small to illustrate on the field map they were illustrated clearly on the actual data, see Figure 14.

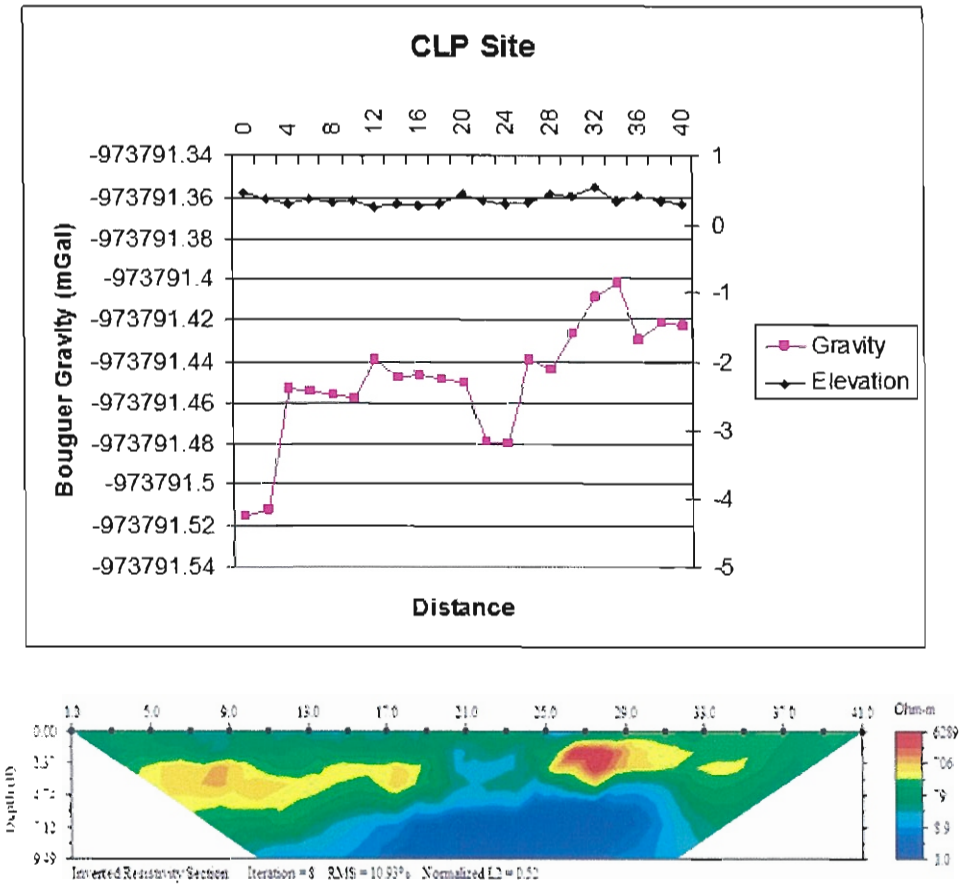

Figure 14 – CMP Micro-Gravity and Electrical Resistivity Data

Both micro-gravity and electrical resistivity was collected at the established two-foot interval spacing. There is a .03 μgal difference depicting the subsurface feature; however, the overall line of collected micro-gravity data does not solely distinguish the storm sewer. On the electrical resistivity traverse the storm sewer is located between electrodes 14 and 15. The storm sewer is roughly at a depth of half to one-foot and has an inside diameter of three-feet with a casing of six-feet. As Figure 14 illustrates the subsurface feature appears relatively big in diameter for its true diameter. Subsequently, the casing surrounding the feature makes the anomaly appear greater than what the true diameter of the storm sewer is.

MI Site

The MI site had the reinforced concrete (RCP) storm sewer. Reinforced concrete is a mixture of metal bars and concrete. This site was located within a basin, which made the casing surrounding the storm sewer appear greater horizontally than vertically. The terrain where the storm sewer was located made it difficult to collect the two separate traverse measurements over the exact same location. Again, as the previous study site the micro-gravity traverse was slightly different than the electrical resistivity traverse. The layout of the MI site is shown in Figure 15.

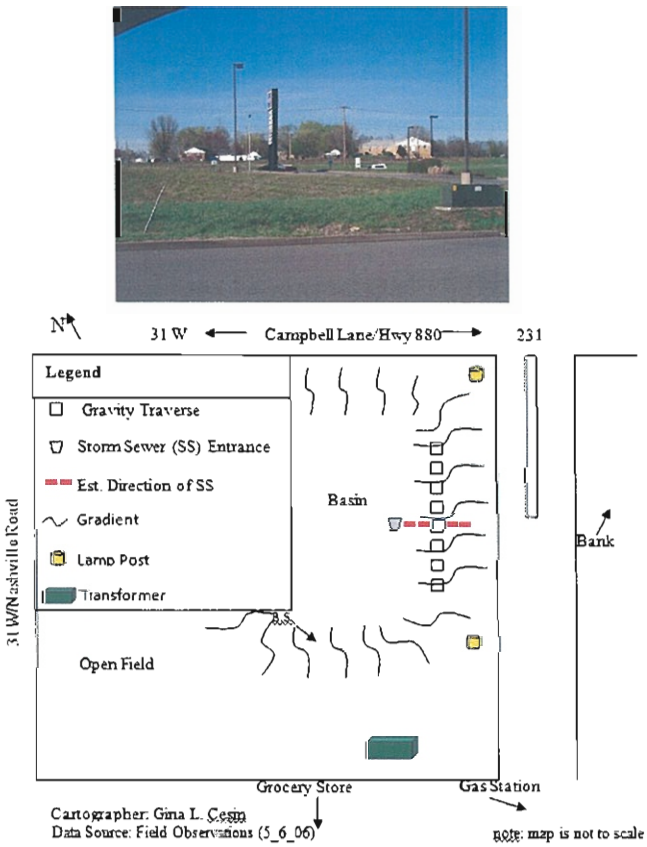

Figure 15 - Reinforced Concrete Pipe Study Site
Source: Field Observations (5_8_06)

Figure 15 illustrates a gradient in which the traverse line was collected. This characteristic of the study site made it particularly more difficult to identify a flat surface

along the traverse where micro-gravity data could be collected. As observed on Figure 16, the storm sewer was identified on the 18th collected point of the micro-gravity traverse.

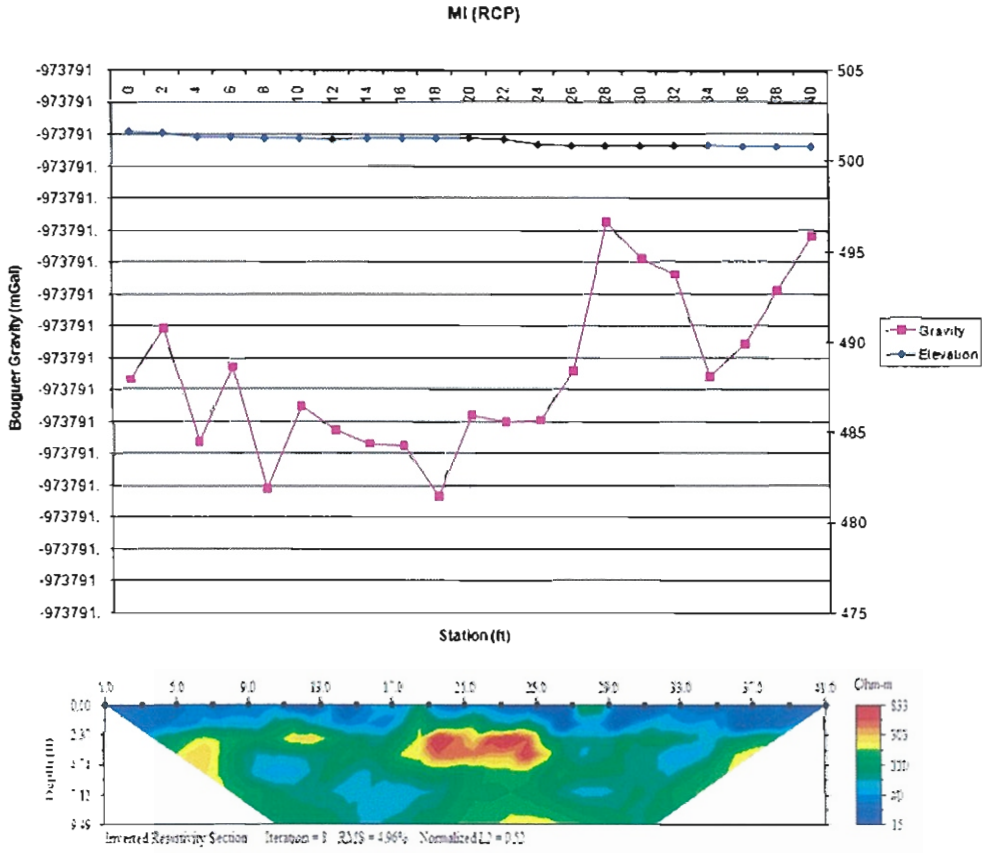

Figure 16 – RCP Micro-Gravity and Electrical Resistivity Data

While the storm sewer had an observed low density the overall gravity traverse does not illustrate an easily observable and outstanding feature. The electrical resistivity traverse depicts the physically observable storm sewer case, unique to this site. Located between the 10th and 13th electrode, the storm sewer is two and a half feet in diameter at a depth of two-feet. Figure 16 illustrates a relatively elongated anomaly 20 to 26ft into the traverse, just as the physical appearance of the storm sewer.

Storm Sewer Conclusion

The storm sewer case studies illustrated that the combination of micro-gravity and electrical resistivity measurements provided the most effective method to identifying a subsurface void of shallow and small diameter. The observations concluded what a subsurface feature of storm sewer characteristics would appear as, and what comparing/contrasting features of commonly used material for storm sewer construction might also appear as. The high-density polyethylene (HDPE) study site determined a two-foot interval spacing for both gravity and electrical resistivity that was applied to the other study sites. The micro-gravity data on the high-density plastic did not provide anything significant; however, the 2 ft interval spacing on electrical resistivity distinctly identifies the feature. The corrugated metal (CMP) and reinforced concrete pipe (RCP) sites provided a challenge in collecting gravity and electrical resistivity measurements. The casing surrounding these two sites was observed through the readings. In addition, the gravity measurements were not directly in-line with the resistivity traverse due to field characteristics. Ultimately, the CMP appeared higher in resistance than the other pipes, while the RCP was much less resistive and the HDPE even more so. This observation appears reasonable, seeing that the CMP has the greatest potential for high porosity. The RCP is then much less resistant because of the conductive metal that is cemented in the formation of the storm sewer. Lastly, the HDPE has the least amount of porous space, making it highly dense. Each feature observed in the modeled data has a unique shape to them. The most effective illustration of a simple modeled storm sewer and not its additional casing is the HDPE.

CHAPTER VI

POTTER PASSAGE

Potter Passage is a natural cave in Bowling Green, Kentucky with tunnel like characteristics. It had previously been known that the cave is of small diameter and has a relatively shallow depth. Objectives for the study included:

- Identifying a natural subsurface feature with tunnel characteristics
- Establishing micro-gravity differences over different portions of the cave with changed approximate depths.

Site characteristics limited methods of observation for gravity and electrical resistivity data. Two separate sections of the field site had traverse lines observed; however, portions of entire traverse lines were paved, preventing the use of electrical resistivity.

Traverse One

Initially, the first traverse of Potter Passage was conducted with both electrical resistivity and micro-gravity. This was the only traverse within this case study that allowed both geophysical techniques to be implemented. Due to the level of uncertainty as to where the actual cave was located an additional micro-gravity survey was conducted, extending the survey site (denoted as Potter Passage Traverse 1a – Figure 17).

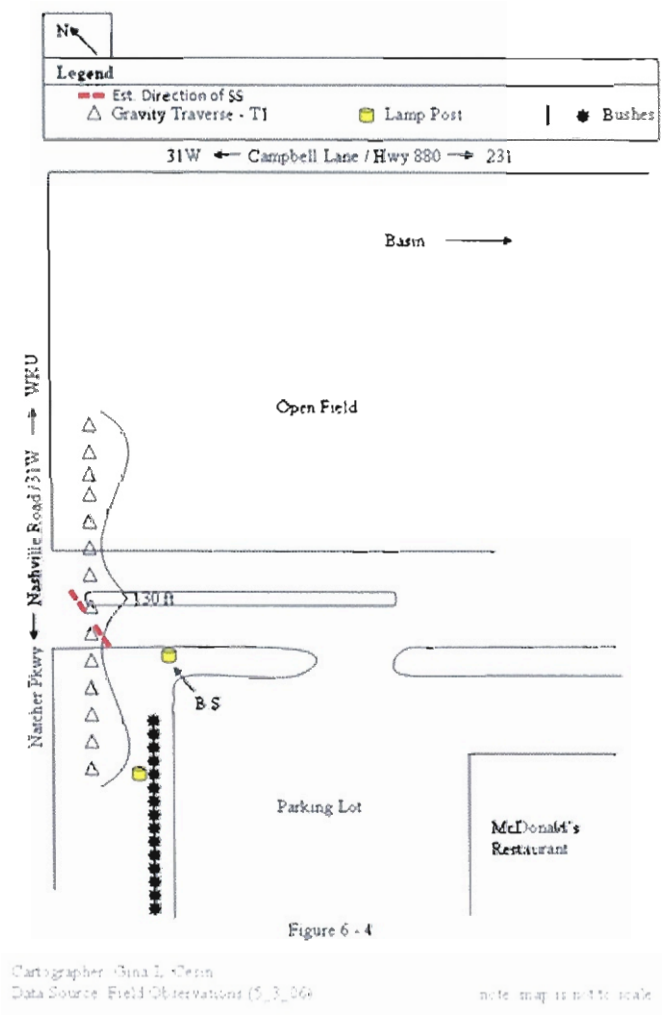

Figure 17 - Potter Passage Traverse 1a Field Map
Source: Field Observations (5_3_06)

The extended survey line begins in-line with the lamp post and extends over the intersection that leads into the shopping plaza. Observed measurements are illustrated in Figures 18 and 19. The electrical resistivity traverse clearly illustrates a highly resistive anomaly, seen in Figure 18. This highly resistive anomaly correlates to the microgravity measurements which illustrate a low gravity anomaly within the same region, also seen in Figure 18. The results of the survey show that there are no significant indications of a low gravity anomaly along the extended survey line other than on the initial Traverse 1.

It is therefore concluded that Potter Passage is most likely located in-line with the lamp post between the McDonald's parking lot and Nashville Road/31W.

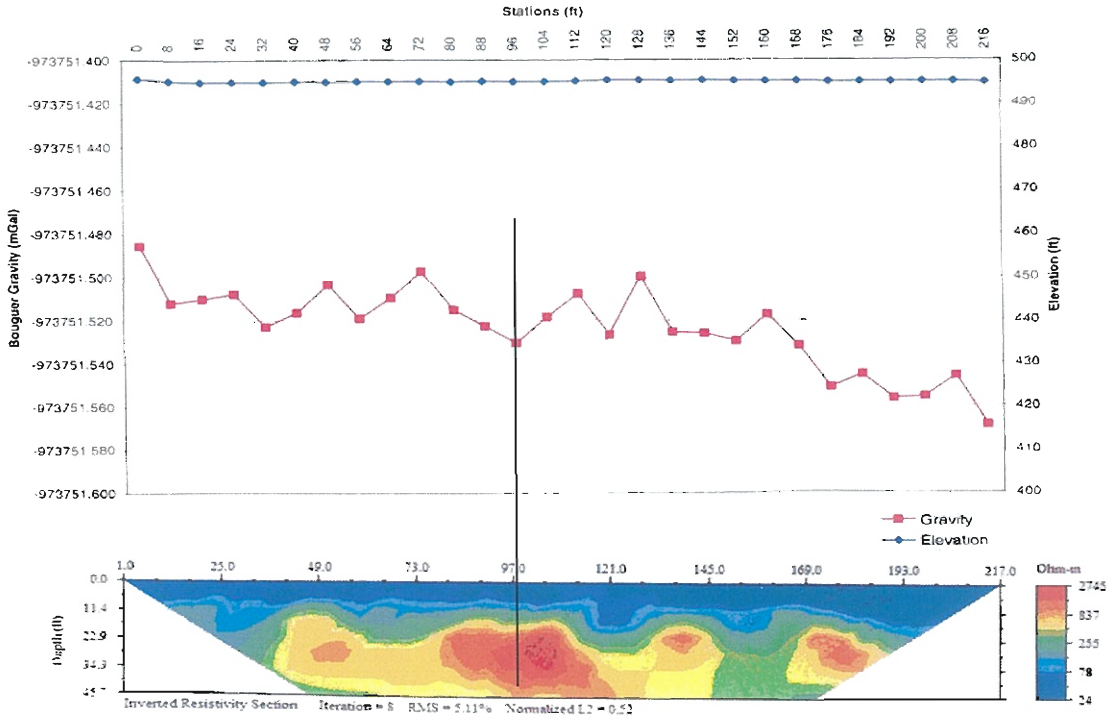

Figure 18 - Potter Passage Traverse 1

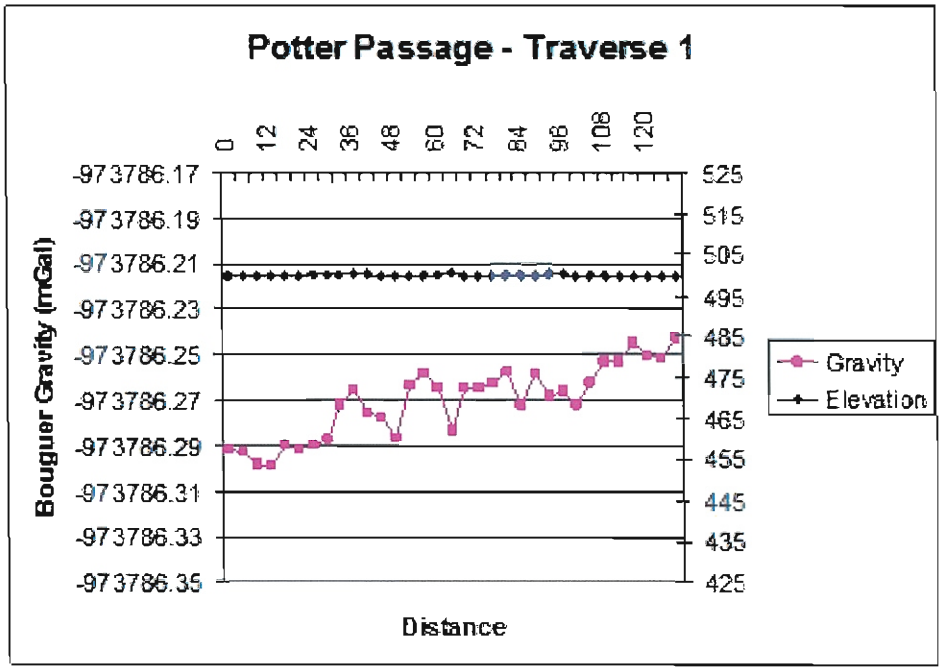

Figure 19 - Potter Passage Traverse 1a

Traverse Two and Three

The second section of Potter Passage that was surveyed was conducted further north of the initial survey. This area of the study is paved and therefore limited to only one geophysical technique, micro-gravity. Again it was uncertain as to the location of Potter Passage in this region, so it was necessary to extend the survey line over a relatively large distance with a small interval spacing, see Figure 20.

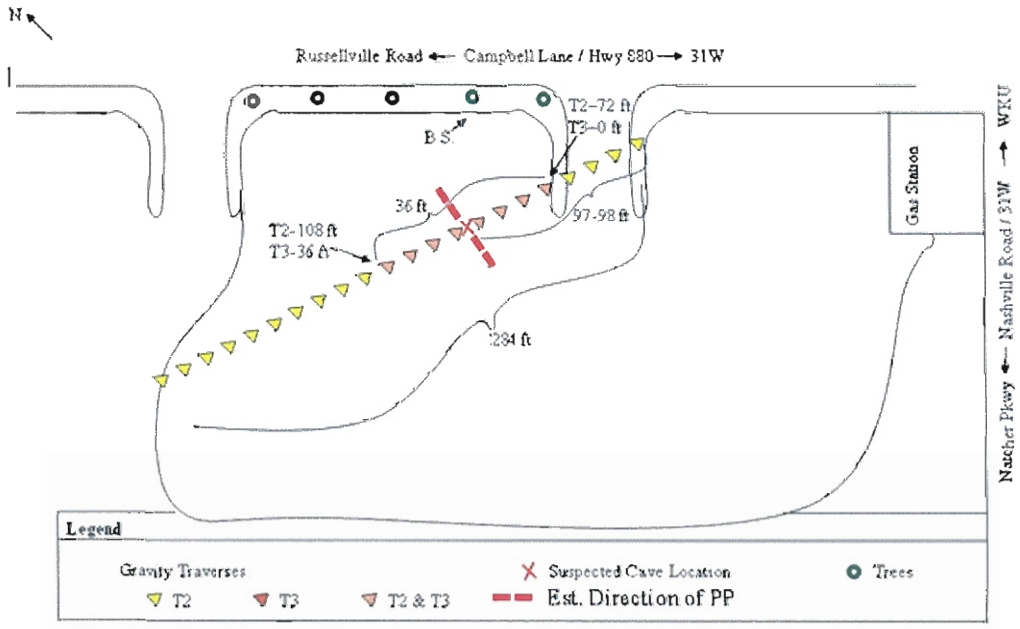

Figure 20 - Potter Passage Traverses 2 and 3 Field Map
Source: (Field Observations 5_6_06 and 5_10_06)

The cave was suspected to be roughly ninety-seven feet into the survey line, but a total of two hundred and eight four feet was surveyed for good measure. Initially, looking at the collected data, it appears as if the survey line completely missed Potter Passage, but a closer look reveals that the cave was most likely just becoming identified in the survey line towards the end of the survey, see Figure 21. The gradual drop in gravity from the suspected cave location to the end of the survey line seems to support this theory. An

additional survey line was conducted over the suspected cave location to verify that there was no low-gravity reading in this region, seen in Figure 22.

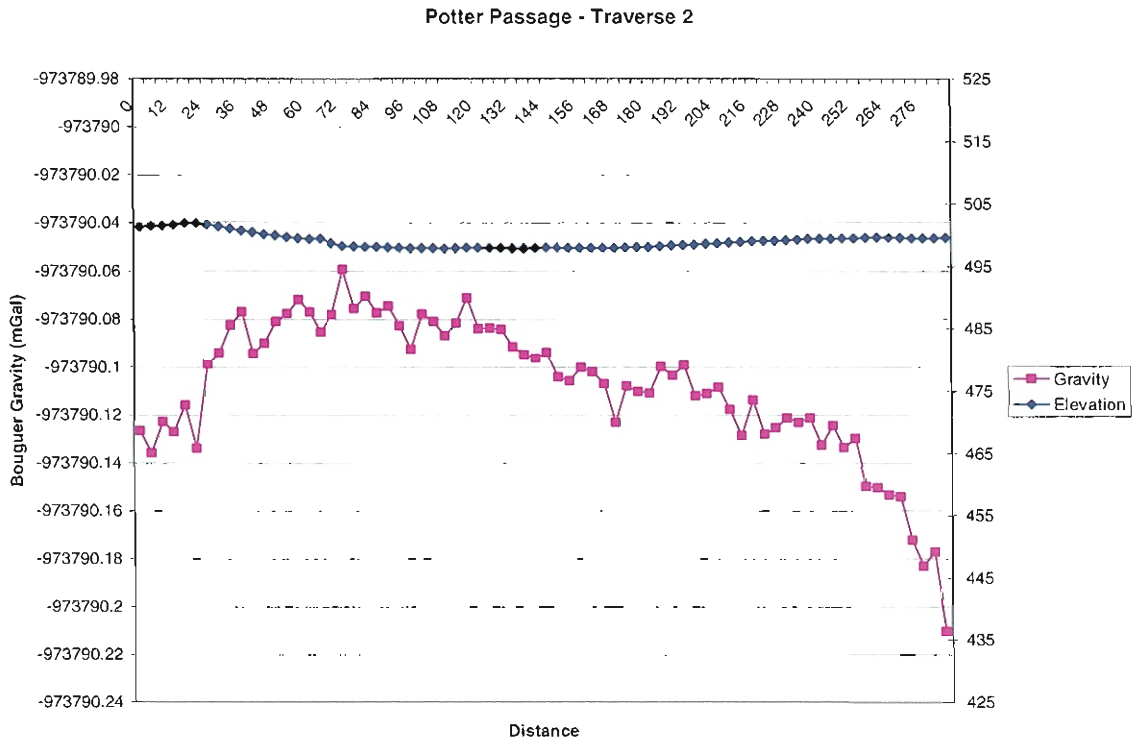

Figure 21 - Potter Passage Traverse 2

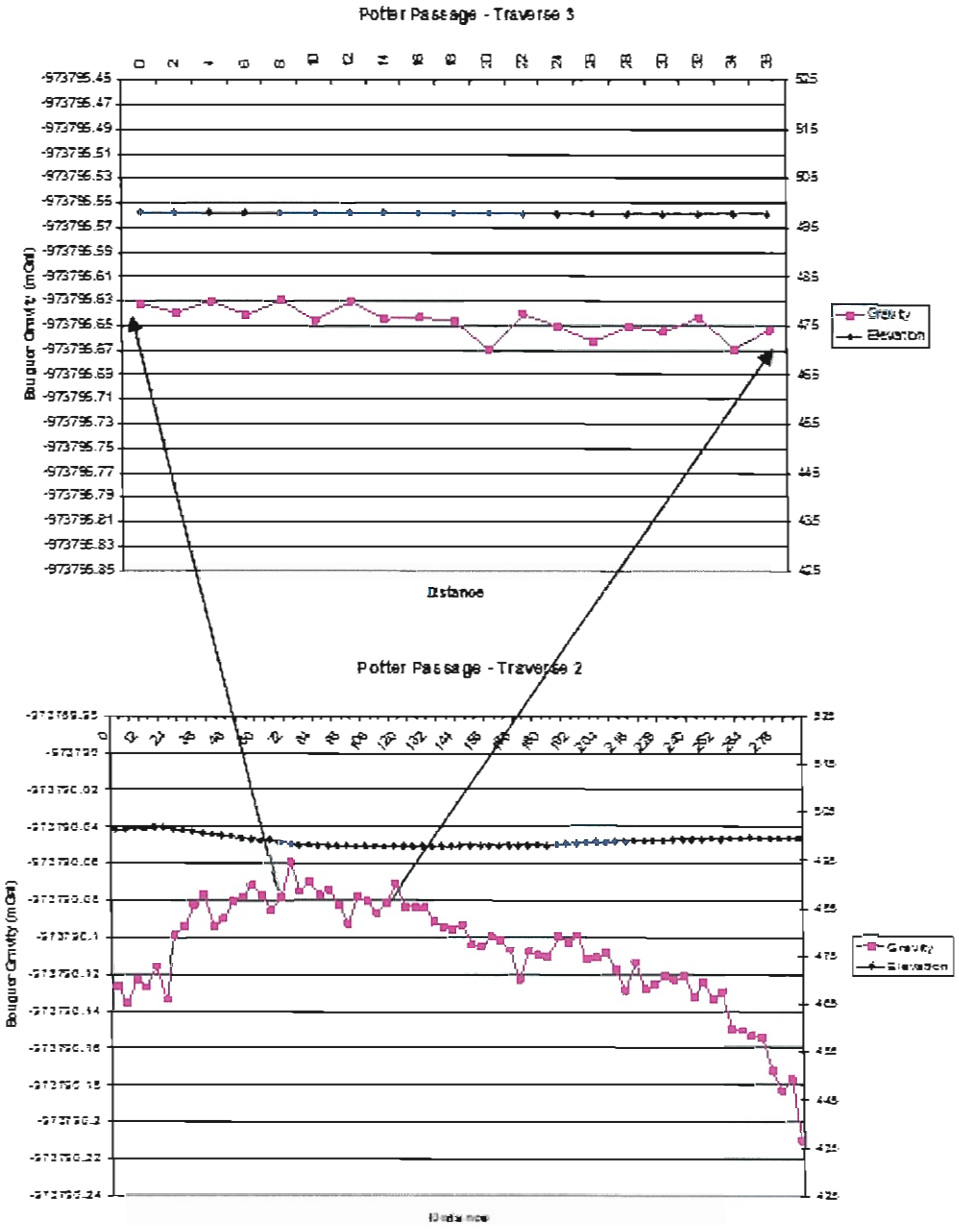

Figure 22 - Potter Passage Traverse 3 Extension of Traverse 2

Potter Passage Conclusion

Based on the collected data the initial survey over Potter Passage did most likely detect the cave at a depth of approximately twenty-three feet, which is consistent with cave radio data collected years earlier. The initial micro-gravity survey correlates with the highly resistive anomaly approximately ninety-eight feet into the survey line (in-line with the lamp post on the field). The extended survey, Potter Passage Traverse 1a, indicates that at the beginning of the survey line (starting in-line with the lamp post) there is a region of low gravity. The second survey site of Potter Passage was conducted over a paved surface that prevented the use of a resistivity survey. The suspected cave location on this site is hypothesized to be disproved. The new suspected cave location is supported by what appears to be a gradually decent of gravity readings towards the end of traverse two. Based on the cave radio data collected years earlier the cave in this region is at an approximate depth of just under fifty feet. This case study was able to identify a natural subsurface feature with tunnel characteristics. In addition, the natural subsurface feature at an approximate depth of twenty-three feet has a μGal difference of 10, while the subsurface feature at an approximate depth of nearly fifty feet has a μGal difference of 35. These μGal difference indicate that there is a void in the subsurface medium.

CHAPTER VII

CLANDESTINE TUNNELS

The clandestine tunnels case study was conducted along the U.S.-Mexico border in Calexico, California. Specifically, there were two study sites within this case study. Site A was the primary site where a total of four traverses were collected back to back. Site B was a secondary site where only one traverse of electrical resistivity was collected in an attempt to collect data on a 4 inch width of soil lined between the border fence and paved asphalt road. The objective of this study included:

- Proving or disproving that the combination of electrical resistivity and micro-gravity will identify clandestine tunnels along the U.S.-Mexico border at Calexico

There were time constraints when collecting data along the border, where a total of four days were used to collect over 800 ft of electrical resistivity data at a two foot interval spacing and over 240 micro-gravity points. The layout of the primary site is shown on Figure 23.

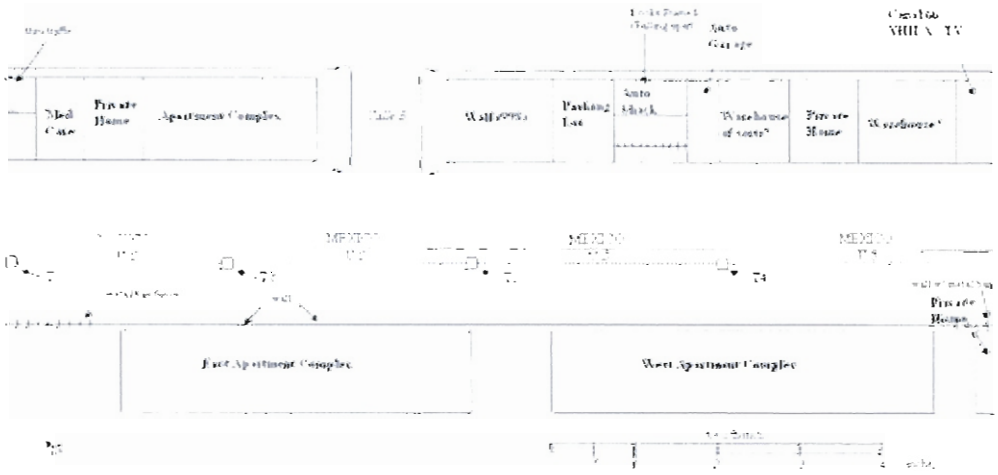

Note: distance is approximated to 69.3 ft/inch.

Figure 23 - Calexico Primary Study Site
Source: (Field Observations 5_19_06 and 5_21_06)

The approach applied to collecting this data included initially obtain electrical resistivity data and then running a micro-gravity survey along portions of the resistivity line that produced resistive anomalies. The base station was located approximately fifty feet off of the survey line in close proximity to a cinder block wall that separates an apartment complex from the border patrolled road.

Site A

Traverse one began at latitude of 32°39'58.2" N and a longitude of -115 °28'37.4" W. Both a resistivity and micro-gravity survey was conducted over the entire survey line that identifies two low gravity relatively high resistive anomalies, see Figure 25. The first combination of low gravity high resistive anomaly is eighty-nine feet into the survey line with a 17 μGal difference, while the second low gravity high resistive anomaly is one hundred and sixty-one feet into the traverse with a 15 μGal difference. The second traverse began at a latitude of 32 °39'58.8" N and a longitude of -115 °28'39.9". At this point gravity surveys were only conducted over regions of high resistivity, see Figure 26. Areas of suspicion range between zero to seventy-two feet and one hundred and four to one hundred and twenty-two feet into the second traverse. There appears to be a μGal difference of 90 twenty-four feet into the first gravity survey line of traverse two. This μGal difference is significantly higher compared to other μGal differences on the survey line and sharply identified among this sections observed points. The second gravity survey of traverse two appears to be a little more complex with several resistive anomalies with corresponding low gravity anomalies. Within this survey there appears to be a total of five possible detections. The first anomaly of the survey is one hundred and

sixteen feet into traverse two with a μGal difference of 10. The second anomaly of the gravity survey line is one hundred thirty feet into the line with a μGal difference of 14. The remaining three anomalies average a μGal difference of 6 and are located one hundred forty eight, one hundred fifty-six, and one hundred and seventy-two feet into traverse two. The electrical resistivity data of traverse three (seen in Figure 27), initiated at a latitude of 32 °39'58.6" N and a longitude of -115 °28'42.4" W, gave notability to a distance between seventy-two to one hundred and ten feet into the traverse. The gravity survey over this section of the traverse appears a bit jagged making it difficult to deduce anything from this region. Traverse four was the final electrical resistivity survey conducted on site one. This traverse, located at a latitude of 32 °39'58.1" N and a longitude of -115 °28'44.7" W, has what appears to be a lot of resistive features (as seen in Figure 28), and even though it would have been preferred to conduct a gravity survey line over the entire traverse it would have been impossible with the time constraints of the case study. Two gravity surveys were performed over this traverse. The first was between thirty and fifty-six feet into the traverse, while the second was conducted between one hundred and forty-eight and two hundred and four feet into the traverse. While the first gravity survey does not appear to have identified a low gravity anomaly, the second gravity survey illustrates two low gravity anomalies that correlate to barely resistive anomalies. The μGal difference of the first low gravity anomaly is 17, one hundred and sixty-four feet into the traverse. The second low gravity anomaly has a μGal difference of 15 at one hundred eighty-four feet into traverse four.

Site B

The Survey Site B was conducted further west of the first Survey Site A, in a region of close proximity to a paved road. Time constraints prevented any gravity measurements from being observed at this site. This resistivity traverse appears to detect no resistive anomalies at depth, see Figure 28. The data points gathered, also seen in Figure 28, illustrate that a large amount of data is missing.

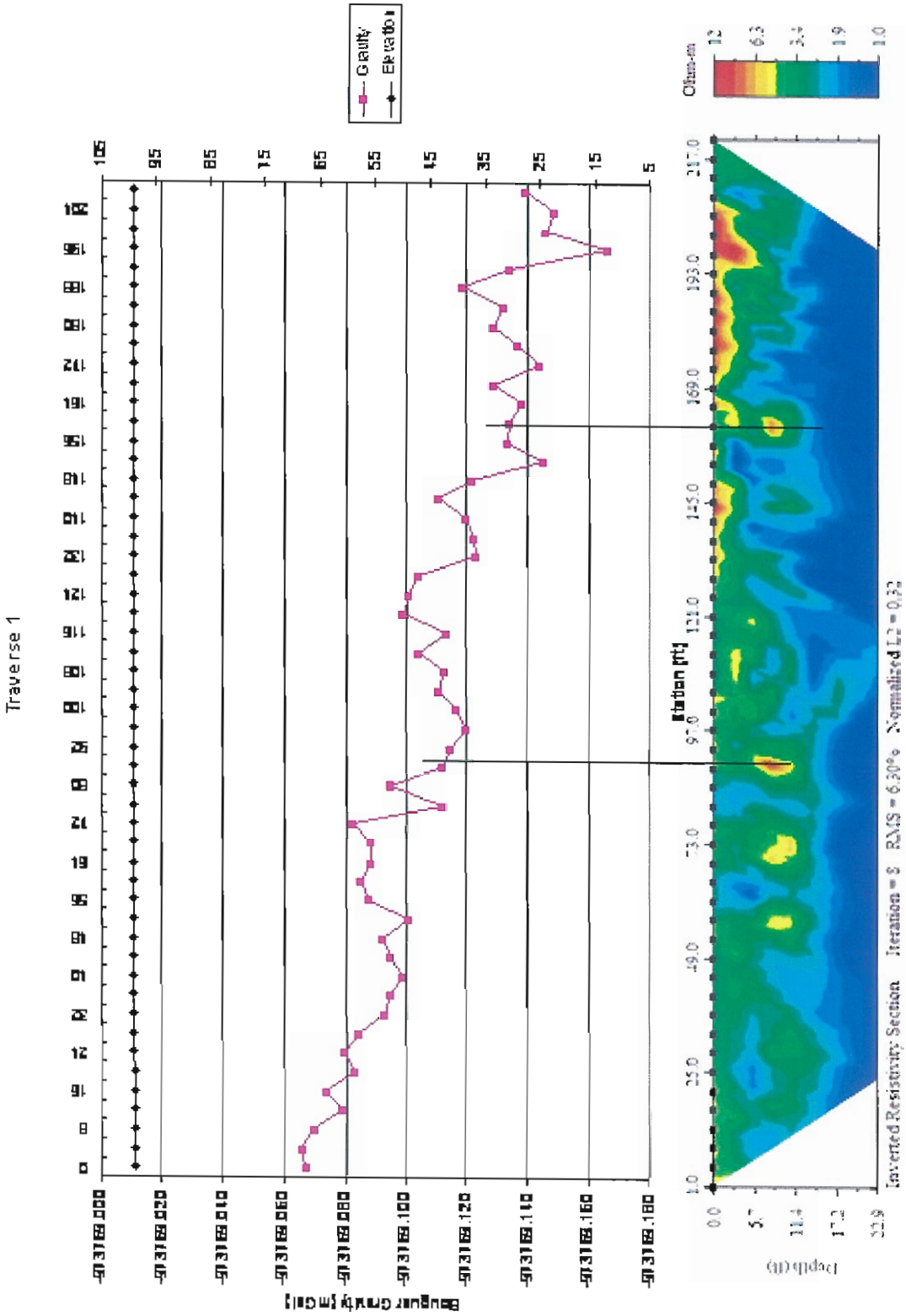

Figure 24 - Clandestine Tunnel Traverse 1

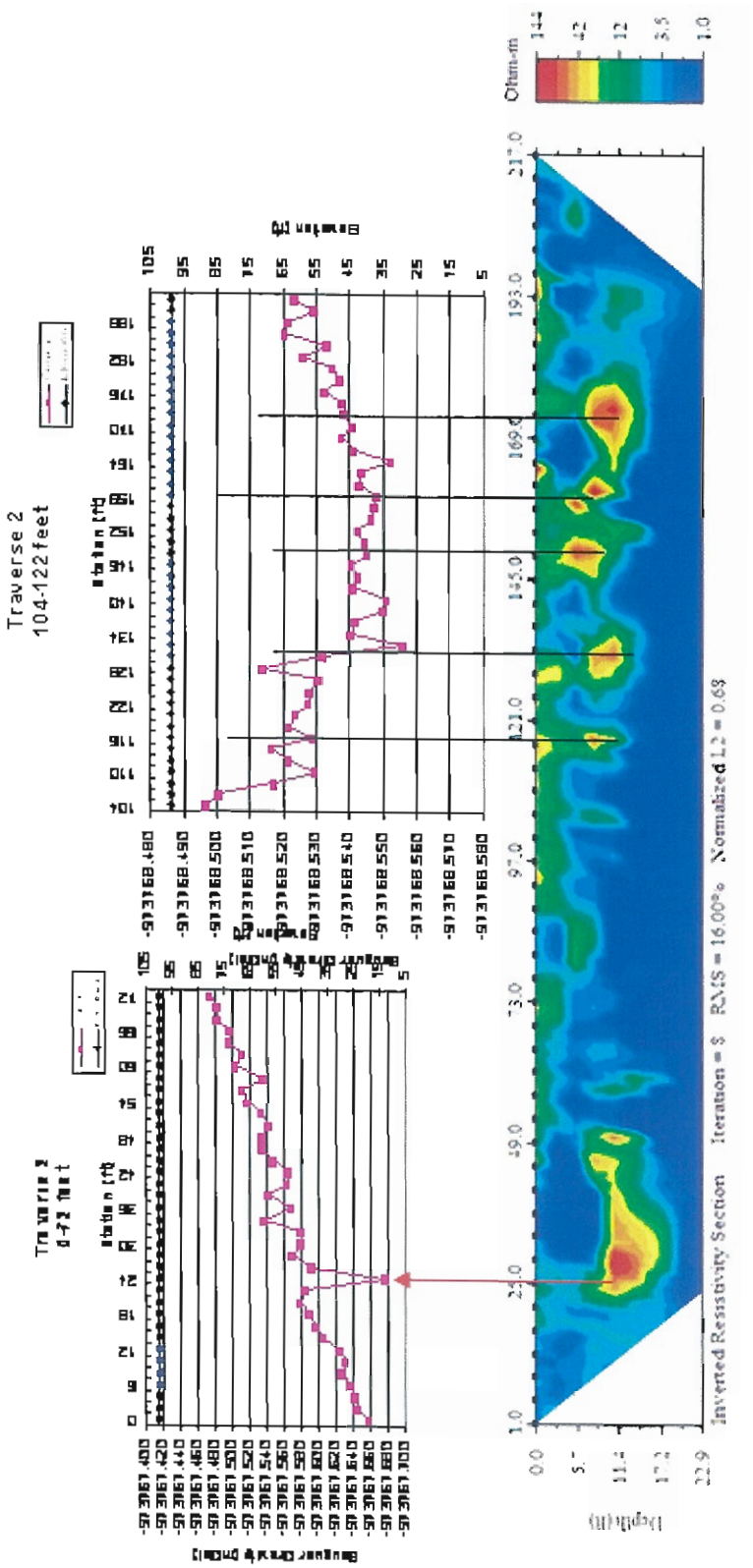

Figure 25 - Clandestine Tunnel Traverse 2

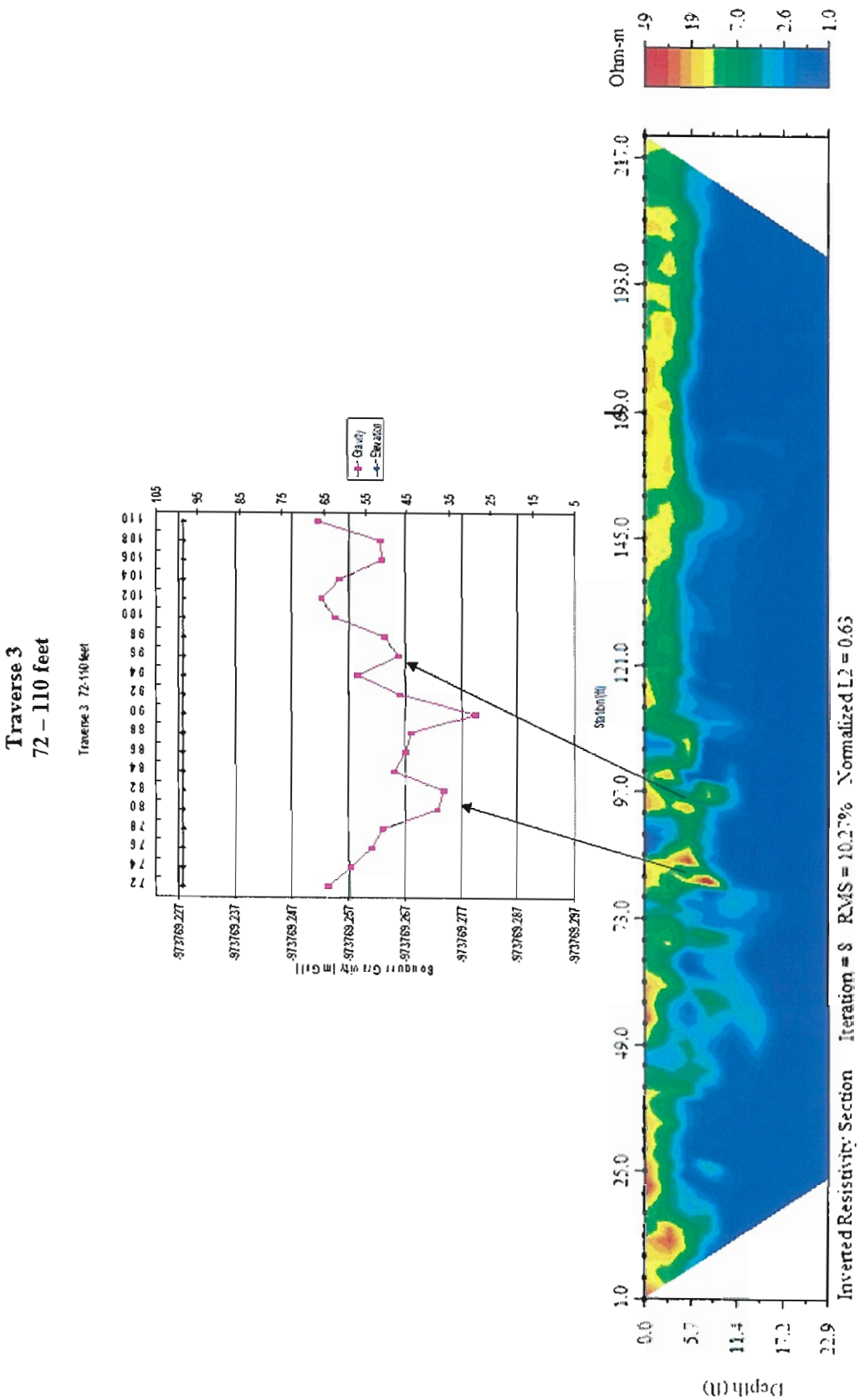

Figure 26 - Clandestine Tunnel Traverse 3

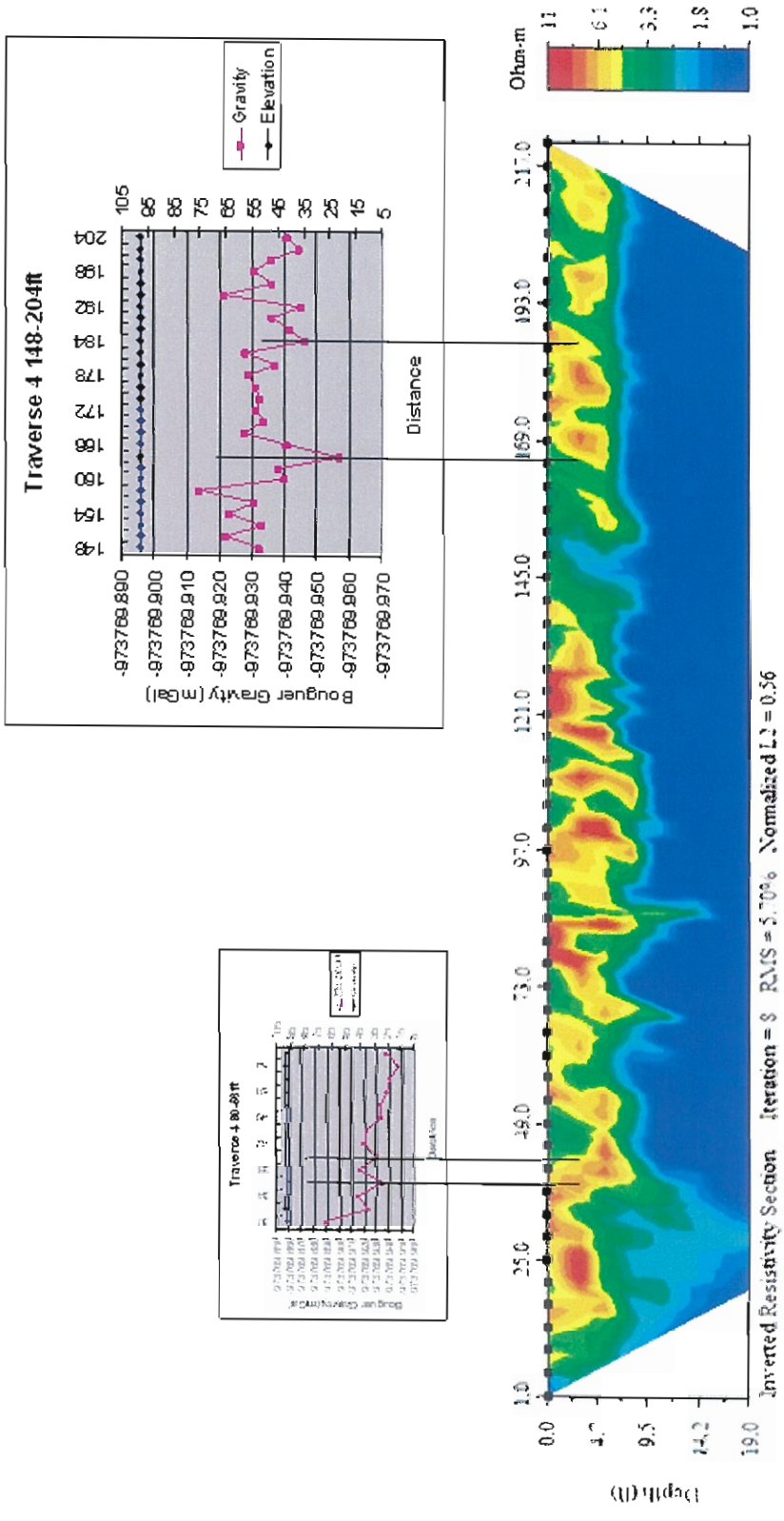

Figure 27 - Clandestine Tunnel Traverse 4

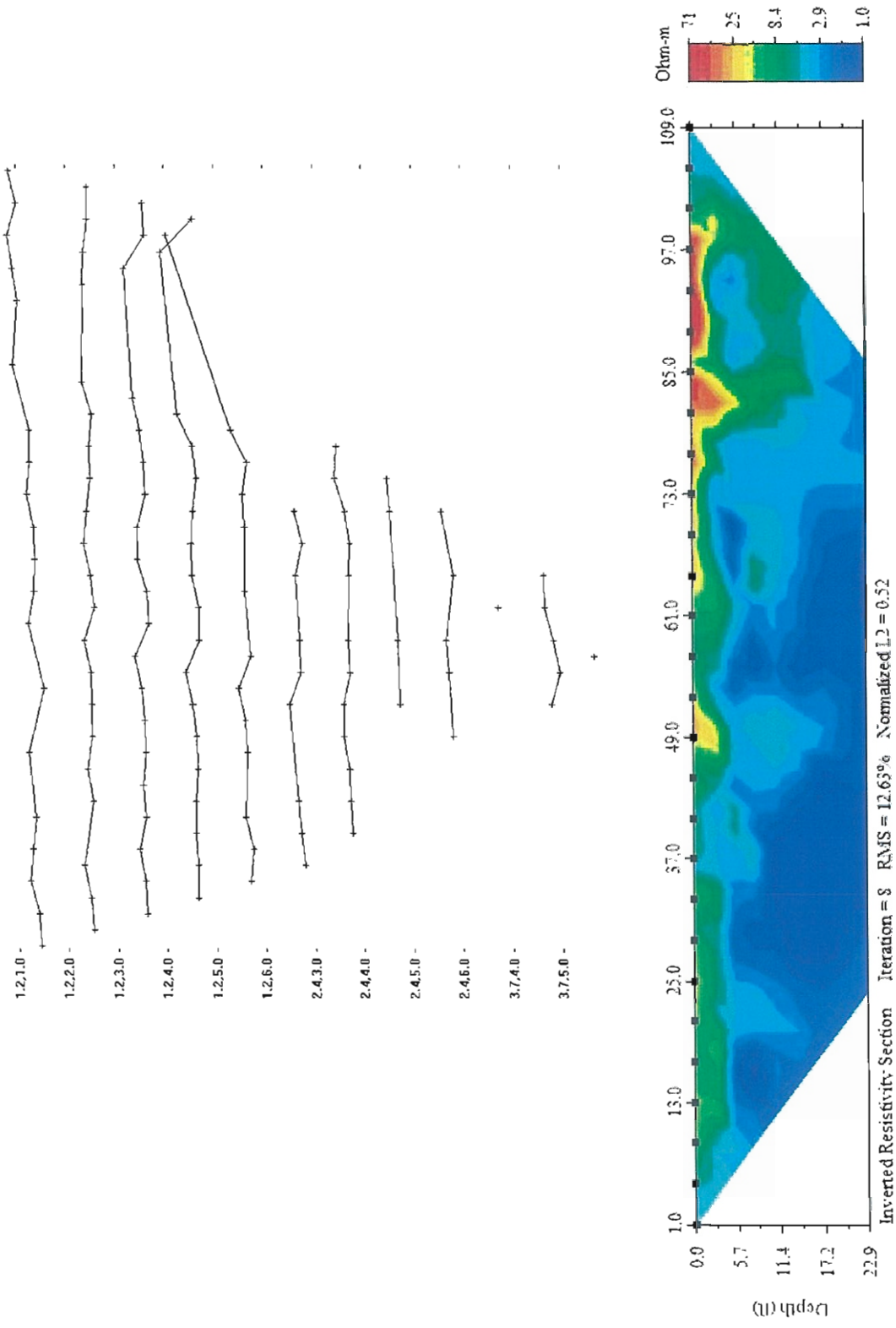

Figure 28 - Clandestine Tunnel Traverse 5 with Acquired Data Points

Clandestine Tunnels Conclusion

The results of the collected data for both electrical resistivity and micro-gravity seem to have identified anomalies. As seen in the resistivity pseudo-sections the area has a high water table that masks any voids within and below it, making it difficult if not impossible to identify. While the water table masks the resistance of the media within it there appears to be some identification of resistive features closer to the surface, above the water table. In addition, micro-gravity data appears jagged and not as smooth as what has been observed in Kentucky. Taking into account what the field conditions where, the large traffic volume on the Mexican side of the border seems to have prevented the collection of more precise data. Even though low gravity readings were jagged and not as smooth as what is accustomed, there is some identification through what was collected. At this point there are only suspected clandestine tunnel locations based on correlating low gravity and high resistivity anomalies collected on Site A. Specifically, there are approximately thirteen anomalies of interest on Site A, see Figure 31. Site B's lack of data does not provide enough or accurate data to make further determinations, and will therefore not be discussed further. On Traverse 1 (Site A) there are two suspected tunnels, while on traverse two there are six suspected tunnels. The initial suspected tunnel off of Traverse 2 has a strong micro-gravity and electrical resistivity signature correlation for a void within a subsurface media. Traverse three appears to have two suspected tunnels, while traverse four has four suspected tunnels. The approximated distance of these suspected tunnels from their respective traverse, depth, and diameter are shown in Table 1.

Traverse	Length into Line (ft)	Depth of Void (ft)
1	89	5
1	158	5
2	24	8.5
2	116	5.5
2	131	6
2	149	3
2	158	3
2	171	7
3	81	5
3	95	6
4	34	2.5
4	40	2.5
4	164	2
4	185	2

Table 1 - Suspected Tunnel Locations

As Figure 31 illustrates there is somewhat of a cluster of suspected tunnels that are perpendicular to Calle B's direction. Initially these suspected locations would seem unreasonable; however, from speaking to ICE agent's clandestine tunnels crossing the border may not necessarily come from a structure at the periphery of a border town, but closer to its center.

CHAPTER VIII

COMPARABLE RESULTS

Conducting a study along the U.S.-Mexico border required the cooperation of U.S. Northern Command. Known tunnel locations were known by U.S. Northern Command prior to the study being conducted; however, these locations weren't provided to the survey team until after collection and analysis of the data. Now that suspected tunnels have been established known tunnel locations can be viewed and compared. Suspected tunnel locations were previously established and are now reading for comparison with the known tunnel locations. The hypothesized location, depth, and diameter of these suspected tunnels are established for comparison. In addition, the hypotheses as to whether these techniques can be proven or disproved to locate clandestine tunnels can be concluded.

Known Tunnel Locations

The three known tunnel locations were provided by U.S. Northern Command. Previously unknown, these tunnel locations are located on Site A within the 828 ft (252 m) electrical resistivity survey line. Each of these tunnels is located within traverse one, two, and three (see Figure 30). In addition, their approximate distance off of the respective traverse is listed in Table 2.

Traverse 1	161 ft into T1
Traverse 2	87.5 ft into T2
Traverse 3	126 ft into T3

Table 2 - Known Tunnel Locations

Two out of three of these tunnels are air filled while the last is water filled. The known tunnel in traverse one, identified in 2005, is the water filled tunnel, and is roughly one hundred and sixty-one feet into the traverse. Traverse two has a known tunnel approximately eighty-seven and a half feet into the traverse. It is provided that this tunnel is an underground culvert feature. The final known tunnel, located in 2003, is located roughly one hundred twenty-six feet into the traverse, as one of the two air filled tunnels.

Comparing Tunnel Locations

Comparing the data collected to the data given, only one of the three known tunnels was actually suspected, see Figure 32. Surprisingly, the tunnel identified is also the water filled and plugged tunnel. The known, but unidentified tunnels are displayed as a feature of average resistance and not highly resistive as what would be expected. These two tunnels were not observed with micro-gravity because of time constraints that prevented entire traverses from being observed, and only allowed highly resistive features be additionally observed.

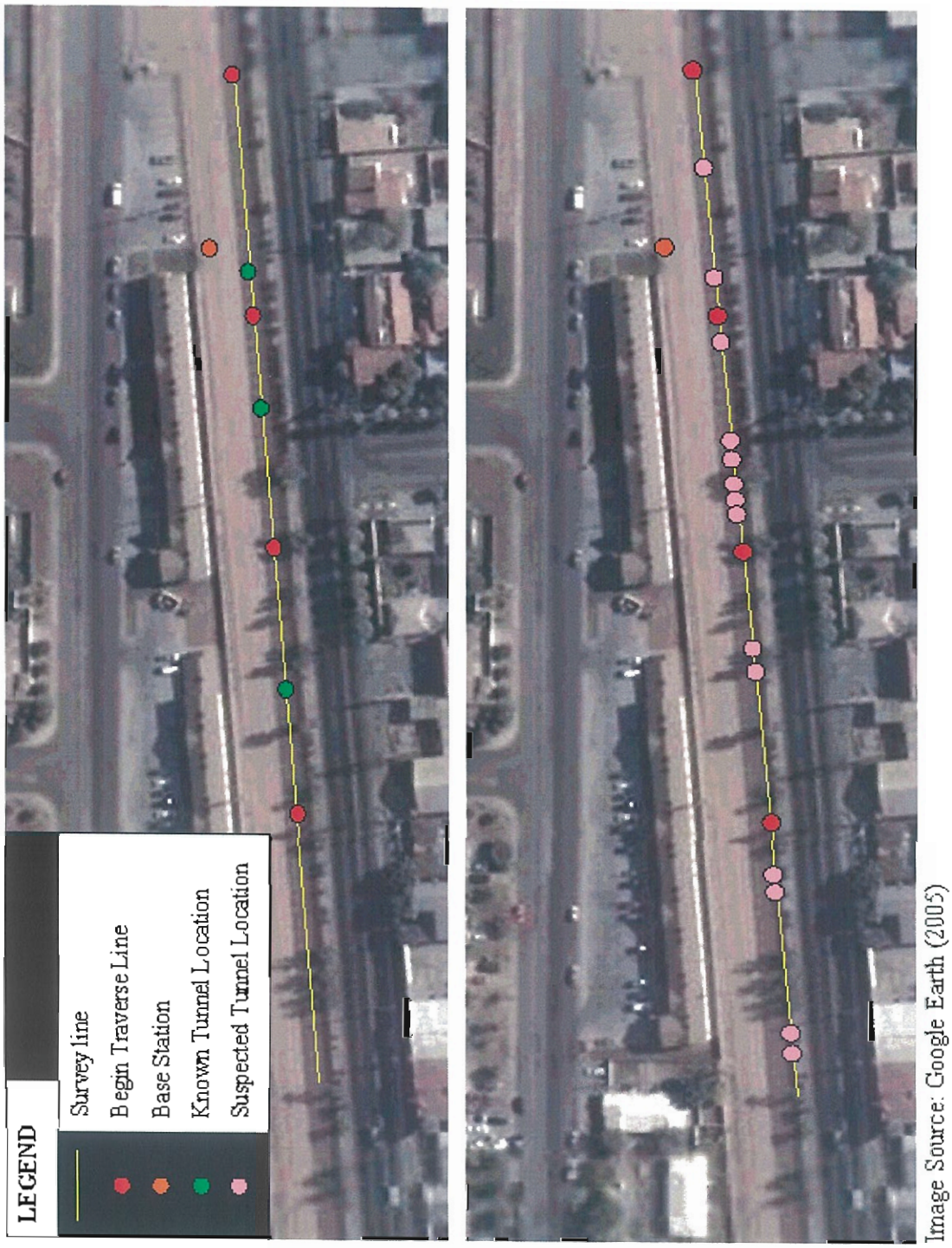

Figure 29 - Known and Suspected Tunnel Location

Figure 30 - Comparing Known and Suspected Tunnel Locations

CHAPTER IX

DISCUSSION

Factors that have influenced this study are cultural noise, subsurface resistance levels, selection of station location, and wind-induced vibration. The clayey lacustrine sediments of the area, combined with the high water table, result in low resistivity value in the subsurface. This setting makes it difficult to identify resistive anomalies because of the amount of conduction available in the subsurface. The electrical current emitted into the ground will follow the path of least resistance and if there is an ample area of conduction the areas of resistance will be to some degree by-passed. In addition, the moisture content, humidity levels, of a void space would reduce the level of resistance of the anomalies. Microgravity graphs (jagged verses smooth) were affected by both wind and traffic-induced vibrations from Mexicali. Typically, when observing gravity readings a standard deviation of the readings should not surpass a reading of .05 mGal for accuracy; however, when unavoidable factors such as heavy winds, tree roots, and subsurface streams are in the path of observation allowances are made for standard deviations of no more than .06 mGals. The Calexico study site was unusual in that gravity readings needed to be observed along a region of high traffic volume, resulting in high standard deviations averaging .09 mGal, see Appendix F. The acceptable standard deviation for this study site was then set at .09 mGal. By decreasing the accuracy of the gravity readings the curves on the graphs were no longer smooth, but jagged which is not what studies from the CCKS are accustomed to observing on traditional gravity graphs. The resistivity traverse on Site B had other factors that affected the observation. Unlike

Site A, Site B was located between the border fence and an asphalt road. The resistivity electrical cables were laid down on the road itself, while the electrodes where placed in close proximity to the border fence. The narrow section of sediment between the parallel road and border fence made it difficult to distance the electrodes from the border fence, and as traverse 5 on Site B depicts it is necessary to not only collect a sufficient amount of data, but good data as well. Such examples of good and bad data points are provided in Appendix G. The data points collected for study Site B were either bad or missing, producing an inaccurate representation of the subsurface.

CHAPTER X

CONCLUSION

The study site at Calexico had poor site conditions in which to prove or disprove the hypothesis that both of these techniques are capable of identifying clandestine tunnels along the U.S.-Mexico border. Because the U.S.-Mexico border is vast and has unique characteristics at each port along the border it is still possible to demonstrate that these geophysical techniques are capable of locating clandestine tunnels along the U.S.-Mexico border. The characteristics on the border at Calexico proved that these techniques have limited suitability at this port of entry. The strong signature correlation between the two geophysical techniques indentified off of Traverse 2 at Site A (yet to be confirmed) provides a strong working theory that these techniques have been proven to work in Calexico, CA. The conclusion of this thesis is that a variety of geophysical techniques will need to be implemented on the U.S.-Mexico border. The characteristics of the individual ports area must be evaluated to establish the most effective geophysical method to identify subsurface voids for each port location on the U.S.-Mexico border. I recommend that the strongly correlated feature identified off of Traverse 2 (Site A) be drill-confirmed to indefinitely prove or disprove these geophysical techniques in Calexico, CA. I recommend that these geophysical techniques be evaluated on a section of the border with dissimilar characteristics to Calexico.

Appendix A – Southern California Geologic Time Scale

Years (m.y.)	Event
.002 (20,000 yrs)	Rain-shadow effect combined with arid climate produces a desert
.5-1	Series of lakes that intermittently occupied the Salton Basin –Lake Cahuilla
.75-1.5	Lacustrine inundations of the Salton Trough
2	Regional desert created due to late Pliocene-Pleistocene elevation, creating huge rain-shadow to the east
2.5	Intensive faulting (uplift and westward lifting) of eastern side of Sierra
4	Colorado Delta spanned the Salton Trough and isolated its northern part from the Gulf of California
4.3-5.5	Initiated incursion of the Colorado River and construction of the Colorado Delta
~ 22	Marine waters occupied nearly all of the trough
30	Earth begins to stretch east to west, modern day basin begins to appear
200	Mountain building event (Basin and Range Province)
560	Bulk of exposed rocks on range laid down on the bottom of a shallow sea (Basin and Range Province)

Source: Morrison (1991)

Appendix B – Salton Trough Fault Zones

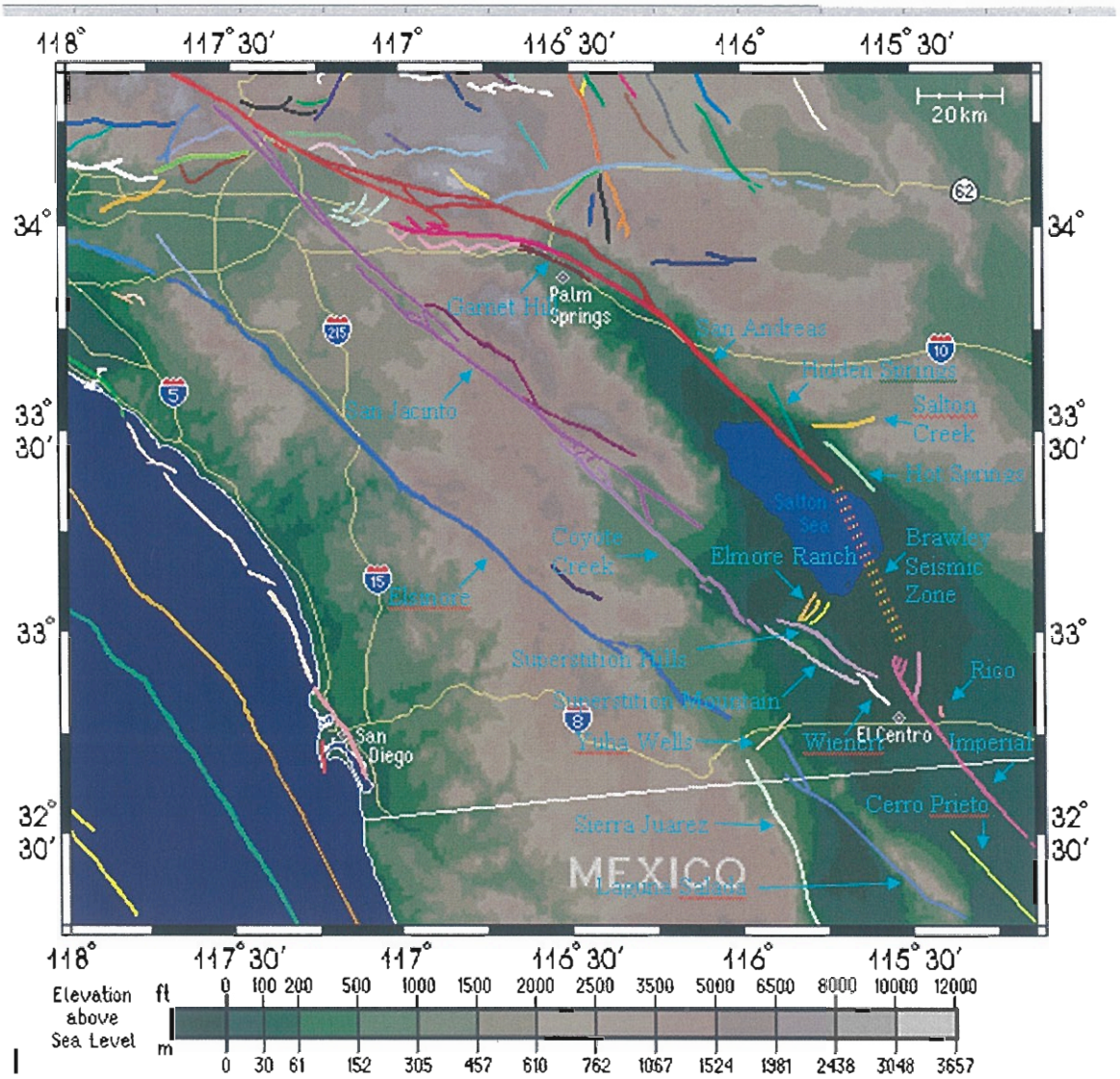

Data Source: Southern California Earthquake Data Center (SCEDC), 2004

Fault Zone	Faulting Type	Length (km)	Slip Rate (mm/yr)	Last Surface Rupture	Probable Magnitude (M_w)
Brawley	right-lateral strike-slip (north-south trending), north-dipping thrust and south-dipping left-lateral and normal (both northeast trending)	15	20 (?)	Jan.-March 1975 & Oct. 1979	< 5-6.5
Brawley Seismic Zone	right-lateral	45	-	-	-
Cerro Prieto	right-lateral	115	uncertain	1934	6.5-7.5
Coyote Creek	right-lateral strike-slip	80	2.0-6.0	Apr. 1968	6.5-7.5
Elmore Ranch	Left-lateral strike-slip	10	.5-1.5	Nov. 1987	5.8-6.5
Elsinore	right-lateral strike-slip	180	4	May_1910	6.5-7.5
Garnet Hill	right-lateral strike-slip	25	10.0-20.0	Late Quaternary/Holocene	6.0-7.0
Hidden Springs	uncertain	20	-	Late Quaternary	-
Hot Springs	right-lateral strike-slip	19	-	Holocene	-
Imperial	right-lateral strike-slip	69	15-20	Oct. 1979 & May 1940	Mw 6.0-6.7 M_w 6.5-7.0
Laguna Salada	right-lateral strike-slip; right-lateral normal oblique	70	4	Feb. 1892	6.5-7.5
Rico	normal	>= 1	-	Oct. 1979	-
Salton Creek	left-later (?)	18	-	Late Quaternary	-
San Andreas	right-lateral strike-slip	1200	20.0-35.0	Jan. 1857 & Apr. 1906	6.8-8.0
San Gorgonio	thrust	35	uncertain	Late Quaternary/Holocene	6.0-7.0 (?)
San Jacinto	right-lateral strike-slip; minor right reversal	210	7.0-17.0	Apr. 1968	6.5-7.5
Sierra Juarez	normal (?)	100	-	Quaternary (?)	-
Superstition Hills	right-lateral strike-slip	30	1.7-5.5	Nov. 1987	6.0-6.8
Superstition Mountain	right-lateral strike-slip	28	5.0-9.0	Late Quaternary/Holocene	6.0-6.8
Wienert	right-lateral strike-slip	10		Nov. 1987	5.5-6.3 & 6-6.8
Yuha Wells	left-lateral (?)	14	-	Late Quaternary	-

Data Source: Southern California Earthquake Data Center (SCEDC), 2004

Appendix C – Electrical Array Lateral Resolutions

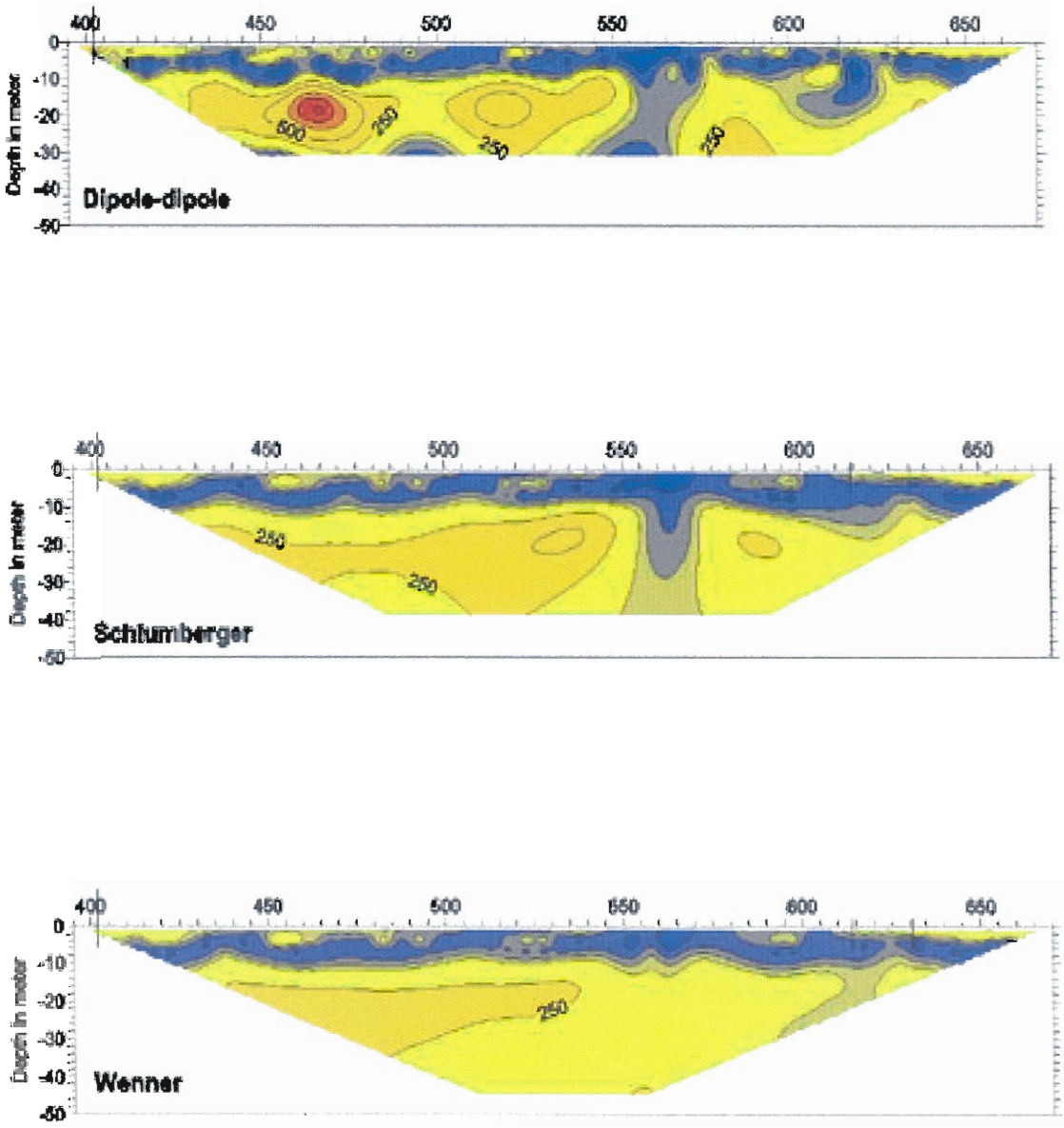

Source: AGI Presentation (2005)

Appendix D – Rock Resistivities

Resistivity of Igneous and Metamorphic Rocks

Rock Type	**Resistivity range (Ωm)**
Granite	$3 \times 10^2 - 10^6$
Granite porphyry	4.5×10^3 (wet) – 1.3×10^6 (dry)
Feldspar porphyry	4×10^3 (wet)
Albite	3×10^2 (wet) – 3.3×10^3 (dry)
Syenite	$10^2 - 10^6$
Diorite	$10^4 - 10^5$
Diorite porphyry	1.9×10^3 (wet) – 2.8×10^4 (dry)
Porphyrite	$10\text{-}5 \times 10^4$ (wet) – 3.3×10^3 (dry)
Carbonatized porphyry	2.5×10^3 (wet) – 6×10^4 (dry)
Quartz porphyry	$3 \times 10^2 - 9 \times 10^5$
Quartz diorite	$2 \times 10^4 - 2 \times 10^6$ (wet) – 1.8×10^5 (dry)
Porphyry (various)	$60 - 10^4$
Dacite	2×10^4 (wet)
Andesite	4.5×10^4 (wet) – 1.7×10^2 (dry)
Diabase porphyry	10^3 (wet) – 1.7×10^5 (dry)
Diabase (various)	$20\text{-}5 \times 10^7$
Lavas	$10^2 - 5 \times 10^4$
Gabbro	$10^3 - 10^6$
Basalt	$10 - 1.3 \times 10^7$ (dry)
Olivine norite	10^3 - 6×10^4 (wet)
Peridotite	3×10^3 (wet) 6.5×10^3 (dry)
Hornfels	8×10^3 (wet) – 6×10^7 (dry)
Schists (calcareous and mica)	$20\text{-}10^4$
Tuffs	2×10^3 (wet) – 10^5 (dry)
Graphite schist	$10 - 10^2$
Slates (various)	$6 \times 10^2 - 4x\ 10^7$
Gneiss (various)	6.8×10^4 (wet) – 3×10^6 (dry)
Marble	$10^2 - 2.5 \times 10^8$ (dry)
Skarn	2.5×10^2 (wet) – 2.5×10^8 (dry)
Quartzites (various)	$10 - 2 \times 10^8$

Source: Telford et al. (1976)

Resistivity of Sediments

Rock Type	**Resistivity range (Ωm)**
Consolidated shales	$20 - 2 \times 10^3$
Argillites	$10 - 8 \times 10^2$
Conglomerates	$2 \times 10^3 - 10^4$
Sandstones	$1 - 6.4 \times 10^8$
Limestones	$50 - 10^7$
Dolomite	$3.5 \times 10^2 - 5 \times 10^3$
Unconsolidated wet clay	20
Marls	3 – 70
Clays	1 - 100
Alluvium and sands	10 – 800
Oil sands	4 - 800

Source: Telford et al. (1976)

Appendix E – Rock Density

Sediments and Sedimentary Rocks

Rock Type	Range	Average (wet)	Range	Average (dry)
	(g/cm^3)		(g/cm^3)	
Alluvium	1.96 – 2.0	1.98	1.5 – 1.6	1.54
Clays	1.63 – 2.6	2.21	1.3 – 2.4	1.70
Glacial drift	-	1.80	-	-
Gravels	1.7 – 2.4	2.0	1.4 – 2.2	1.95
Loess	1.4 – 1.93	1.64	0.75 – 1.6	1.20
Sand	1.7 – 2.3	2.0	1.4 – 1.8	1.60
Sands and Clays	1.7 – 2.5	2.1	-	-
Silt	1.8 – 2.2	1.93	1.2 – 1.8	1.43
Soils	1.2 – 2.4	1.92	1.0 – 2.0	1.46
Sandstones	1.61 – 2.76	2.35	1.6 – 2.68	2.24
Shales	1.77 – 3.2	2.40	1.56 – 3.2	2.10
Limestones	1.93 – 2.90	2.55	1.74 – 2.76	2.11
Dolomite	2.28 – 2.90	2.70	2.04 – 2.54	2.30

Source: Telford et al. (1976)

Metamorphic Rocks

Rock Type	Range	Average
	(g/cm^3)	
Quartzite	2.5 – 2.70	2.60
Schists	2.39 – 2.9	2.64
Graywacke	2.6 – 2.7	2.65
Granulite	2.52 – 2.73	2.65
Phyllite	2.68 – 2.80	2.74
Marble	2.6 – 2.9	2.75
Quartzitic slate	2.63 – 2.91	2.77
Serpentine	2.4 – 3.10	2.78
Slate	2.7 – 2.9	2.79
Gneiss	2.59 – 3.0	2.80
Chloritic slate	2.75 – 2.98	2.87
Amphibolite	2.90 – 3.04	2.96
Eclogite	3.2 – 3.54	3.37
Metamorphic (av.)	2.4 – 3.1	2.74

Source: Telford et al. (1976)

Igneous Rocks

Rock Type	**Range**	**Average**
	(g/cm^3)	
Rhyolite glass	2.20 – 2.28	2.24
Obsidian	2.2 – 2.4	2.30
Vitrophyre	2.36 – 2.53	2.44
Rhyolite	2.35 – 2.70	2.52
Dacite	2.35 – 2.8	2.58
Phonolite	2.45 – 2.71	2.59
Trachyte	2.42 – 2.8	2.60
Andesite	2.4 – 2.8	2.61
Nephelite – Syenite	2.53 – 2.70	2.61
Granite	2.50 – 2.81	2.64
Granodiorite	2.67 – 2.79	2.73
Porphyry	2..60 – 2.89	2.74
Syenite	2.60 – 2.95	2.77
Anorthosite	2.64 – 2.94	2.78
Quartz diorite	2.62 – 2.96	2.79
Diorite	2.72 – 2.99	2.85
Lavas	2.80 – 3.0	2.90
Diabase	2.50 – 3.20	2.91
Essexite	2.69 – 3.14	2.91
Norite	2.70 – 3.24	2.92
Basalt	2.70 – 3.30	2.99
Gabbro	2.70 – 3.50	3.03
Hornblende – Gabbro	2.98 – 3.18	3.08
Periodotite	2.78 – 3.37	3.15
Pyroxenite	2.93 – 3.34	3.17
Acid Igneous (av.)	2.30 – 3.11	2.61
Basic Igneous (av.)	2.09 – 3.17	2.79

Source: Telford et al. (1976)

Appendix F – Clandestine Tunnels Gravity Text

Traverse 1

SCINTREX V5.2 AUTOGRAV / Field Mode R5.21

Line: 3. Grid: 0. Job: 1. Date: 06/05/20 Ser No: 711415. Operator: 1.

GREF.:	0. mGals	Tilt x sensit.:	268.6
GCAL.1:	6187.411	Tilt y sensit.:	261.8
GCAL.2:	0.0	Deg.Latitude:	32.67
TEMPCO.:	-0.1260 mGal/mK	Deg.Longitude:	115.5
Drift const.:	1.77	GMT Difference:	7.hr
Drift Correction Start	Time: 15:35:33	Cal.after x samples:	999
	Date: 06/03/02	On-Line Tilt Corrected = "*"	

Station	Grav.	SD.	Tilt x	Tilt y	Temp.	E.T.C.	Dur	# Rej	Time
0.	5763.232*	0.108	-2.	15.	3.00	0.018	60	0	08:00:16
0.	5763.216*	0.090	-3.	6.	3.00	0.018	60	0	08:02:17
0.	5763.200*	0.092	2.	1.	3.00	0.018	60	0	08:04:38
0.	5763.203*	0.088	3.	4.	3.00	0.018	60	0	08:06:01
4.	5763.184*	0.103	-0.	-1.	3.00	0.018	60	0	08:10:12
4.	5763.194*	0.098	-5.	3.	3.00	0.018	60	0	08:12:01
8.	5763.196*	0.119	-3.	2.	3.00	0.018	60	0	08:14:54
8.	5763.190*	0.094	-5.	4.	3.00	0.018	60	0	08:16:19
12.	5763.174*	0.081	0.	1.	3.00	0.018	60	0	08:19:22
16.	5763.172*	0.081	-1.	1.	3.00	0.018	60	0	08:22:05
20.	5763.167*	0.112	-3.	4.	3.00	0.018	60	0	08:25:14
20.	5763.156*	0.080	-1.	1.	3.00	0.018	60	0	08:26:47
24.	5763.148*	0.084	4.	-2.	3.00	0.018	60	0	08:31:17
24.	5763.146*	0.109	-1.	-1.	3.00	0.018	60	0	08:37:43
24.	5763.152*	0.093	0.	1.	3.00	0.018	60	0	08:39:09
28.	5763.190*	0.000	-1.	-4.	3.00	0.018	1	0	08:35:02
28.	5763.146*	0.122	0.	2.	3.00	0.017	60	0	08:42:09
28.	5763.150*	0.110	-1.	6.	3.00	0.017	60	0	08:43:32
28.	5763.138*	0.124	-3.	-2.	3.00	0.017	60	0	08:45:13
28.	5763.132*	0.115	-4.	-1.	3.00	0.017	60	0	08:46:36
28.	5763.140*	0.103	-3.	-0.	3.00	0.017	60	0	08:48:02
32.	5763.126*	0.098	-1.	-0.	3.00	0.017	60	0	08:51:21
36.	5763.124*	0.114	2.	1.	3.00	0.017	60	0	08:54:20
36.	5763.121*	0.089	3.	1.	3.00	0.016	60	0	08:55:43
40.	5763.114*	0.111	-3.	1.	3.00	0.016	60	0	08:58:34
40.	5763.110*	0.087	-2.	3.	3.00	0.016	60	1	09:00:57
44.	5763.109*	0.173	-4.	3.	3.00	0.016	46	0	09:03:58
44.	5763.110*	0.077	-3.	4.	3.00	0.016	60	0	09:05:03
48.	5763.105*	0.083	-7.	4.	3.00	0.015	60	0	09:08:07
52.	5763.096*	0.102	-4.	-5.	3.00	0.015	60	0	09:11:18
56.	5763.099*	0.114	1.	5.	3.00	0.014	60	0	09:14:26
56.	5763.106*	0.092	1.	5.	3.00	0.014	60	0	09:15:47
60.	5763.103*	0.090	-0.	2.	3.00	0.013	60	0	09:19:36
64.	5763.096*	0.093	-8.	1.	3.00	0.013	60	0	09:22:31
68.	5763.095*	0.095	-2.	0.	3.00	0.013	60	0	09:25:25
72.	5763.087*	0.108	-5.	3.	3.00	0.012	60	0	09:29:21
72.	5763.081*	0.147	-8.	3.	3.00	0.012	45	0	09:30:50
72.	5763.079*	0.152	-0.	3.	3.00	0.012	45	0	09:31:58
72.	5763.090*	0.093	0.	4.	3.00	0.012	60	0	09:33:03
76.	5763.074*	0.119	-2.	2.	3.00	0.011	55	0	09:35:54
76.	5763.065*	0.116	-3.	1.	3.00	0.011	60	0	09:37:16
76.	5763.056*	0.103	-4.	1.	3.00	0.011	60	0	09:38:44
80.	5763.067*	0.099	-4.	3.	3.00	0.010	60	0	09:43:01
84.	5762.944*	0.391	-4.	-3.	3.00	0.009	15	0	09:45:59
84.	5763.058*	0.109	-2.	-2.	3.00	0.009	60	0	09:46:33
84.	5763.061*	0.099	-1.	-4.	3.00	0.009	60	0	09:47:58
84.	5758.630*	0.000	0.	0.	0.00	0.007	1	0	09:56:56
88.	5763.026*	0.107	6.	-0.	3.00	0.007	60	0	09:57:29
88.	5763.025*	0.101	-2.	3.	3.00	0.007	60	0	09:59:42
92.	5758.721*	0.000	0.	0.	0.00	0.006	1	0	10:03:32
92.	5763.017*	0.092	-5.	7.	3.00	0.006	60	0	10:03:45
96.	5763.007*	0.087	-7.	-3.	3.00	0.005	60	0	10:07:08
100.	5763.007*	0.082	-8.	-2.	3.00	0.005	60	0	10:10:15
104.	5762.999*	0.153	-9.	0.	3.00	0.004	40	2	10:13:40
104.	5762.991*	0.106	-4.	1.	3.00	0.004	60	0	10:14:46
104.	5763.001*	0.091	-5.	2.	3.00	0.003	60	0	10:16:11

104.	5763.001*	0.091	-5.	2.	3.00	0.003	60	0 10:16:11
108.	5762.999*	0.090	-4.	0.	3.00	0.003	60	0 10:19:13
112.	5763.002*	0.090	-7.	-3.	3.00	0.002	60	0 10:22:13
116.	5762.987*	0.100	-5.	-4.	3.00	0.001	60	0 10:26:09
120.	5763.011*	0.114	-2.	5.	3.00	0.001	60	0 10:29:06
120.	5762.994*	0.073	-2.	6.	3.00	0.000	60	0 10:30:33
124.	5762.989*	0.084	-3.	2.	3.00	-0.001	60	0 10:33:36
128.	5762.977*	0.128	-5.	-0.	3.00	-0.001	54	0 10:37:48
128.	5762.963*	0.224	-6.	-1.	3.00	-0.002	14	0 10:39:12
128.	5762.973*	0.081	-5.	-3.	3.00	-0.002	60	0 10:40:19
9000.	5762.914*	0.062	-3.	-11.	3.00	-0.006	60	0 11:00:49
9000.	5762.918*	0.060	1.	-8.	3.00	-0.007	60	0 11:02:28
128.	5763.005*	0.082	-3.	14.	3.00	-0.007	60	0 11:06:02
132.	5762.981*	0.104	2.	-2.	3.00	-0.008	60	0 11:08:31
132.	5762.972*	0.115	3.	0.	3.00	-0.008	60	0 11:09:54
132.	5762.980*	0.107	4.	1.	3.00	-0.008	60	1 11:11:19
132.	5762.987*	0.107	4.	2.	3.00	-0.009	60	0 11:12:42
132.	5762.981*	0.084	1.	5.	3.00	-0.009	60	2 11:14:05
136.	5762.977*	0.105	1.	-2.	3.00	-0.009	60	0 11:16:14
136.	5762.979*	0.099	3.	-1.	3.00	-0.009	60	0 11:17:37
140.	5762.981*	0.103	6.	-2.	3.00	-0.010	60	0 11:19:58
144.	5762.990*	0.091	-7.	6.	3.00	-0.010	60	0 11:22:21
148.	5762.979*	0.107	5.	7.	3.00	-0.011	60	0 11:24:43
148.	5762.978*	0.087	-2.	0.	3.00	-0.011	60	0 11:26:14
152.	5762.956*	0.084	-1.	0.	3.00	-0.011	60	0 11:28:50
156.	5762.972*	0.099	-4.	3.	3.00	-0.012	60	0 11:31:03
160.	5762.971*	0.102	1.	2.	3.00	-0.012	60	0 11:33:49
160.	5762.957*	0.089	0.	1.	3.00	-0.013	60	0 11:35:11
164.	5762.950*	0.137	1.	-1.	3.00	-0.013	49	1 11:37:12
164.	5762.959*	0.143	1.	-1.	3.00	-0.013	46	0 11:38:17
164.	5762.952*	0.081	2.	-1.	3.00	-0.014	60	0 11:43:01
168.	5762.969*	0.084	0.	2.	3.00	-0.014	60	0 11:45:41
172.	5762.961*	0.132	5.	-2.	3.00	-0.015	57	0 11:48:04
172.	5762.954*	0.087	11.	-0.	3.00	-0.015	60	1 11:49:17
176.	5762.948*	0.114	-1.	-2.	3.00	-0.015	55	0 11:52:50
176.	5762.952*	0.080	-1.	4.	3.00	-0.016	60	0 11:54:05
180.	5762.959*	0.091	0.	0.	3.00	-0.016	60	0 11:57:15
184.	5762.953*	0.100	4.	-2.	3.00	-0.016	60	0 12:00:08
188.	5762.957*	0.114	-1.	3.	3.00	-0.017	60	0 12:02:57
188.	5762.966*	0.072	1.	3.	3.00	-0.017	60	0 12:04:25
192.	5762.950*	0.103	-2.	7.	3.00	-0.017	60	0 12:07:25
192.	5762.868*	0.076	-1.	-3.	3.00	-0.018	8	1 12:11:30
196.	5762.918*	0.218	1.	-5.	3.00	-0.018	41	1 12:13:42
196.	5762.930*	0.118	0.	-5.	3.00	-0.018	60	0 12:14:51
196.	5762.921*	0.127	-2.	-6.	3.00	-0.018	48	0 12:16:23
196.	5762.917*	0.089	-0.	-8.	3.00	-0.018	60	0 12:17:30
198.	5762.935*	0.089	-0.	-4.	3.00	-0.018	19	0 12:12:00
200.	5758.506*	0.000	0.	0.	0.00	-0.019	1	0 12:19:06
200.	5758.506*	0.000	0.	0.	0.00	-0.019	1	0 12:19:20
200.	5762.937*	0.108	-1.	3.	3.00	-0.019	60	0 12:22:16
200.	5762.937*	0.110	-1.	5.	3.00	-0.019	60	0 12:23:40
200.	5762.930*	0.105	-3.	-2.	3.00	-0.019	60	0 12:25:32
200.	5762.935*	0.086	-3.	0.	3.00	-0.019	60	0 12:27:09
204.	5762.938*	0.132	-0.	3.	3.00	-0.019	60	0 12:30:08
204.	5762.922*	0.115	2.	1.	3.00	-0.020	60	0 12:31:39
204.	5762.930*	0.109	3.	-1.	3.00	-0.020	60	0 12:33:07
204.	5762.930*	0.094	3.	-1.	3.00	-0.020	60	0 12:34:35
208.	5762.932*	0.101	3.	11.	3.00	-0.020	60	0 12:37:00
212.	5762.932*	0.121	4.	-0.	3.00	-0.020	60	0 12:39:31
212.	5762.928*	0.137	4.	1.	3.00	-0.020	60	0 12:40:54
212.	5759.048*	0.000	-2.	2.	3.00	-0.020	1	0 12:42:21
9000.	5763.118*	0.058	-3.	-2.	3.00	0.017	60	0 07:48:34
9000.	5763.123*	0.060	-2.	-2.	3.00	0.017	60	0 07:50:02
9000.	5763.127*	0.052	-0.	-1.	3.00	0.017	60	0 07:51:25
9000.	5763.122*	0.058	2.	-1.	3.00	0.018	60	0 07:53:02
9000.	5763.129*	0.061	3.	1.	3.00	0.018	60	0 07:54:26
9000.	5763.123*	0.053	2.	2.	3.00	0.018	60	0 07:56:28
9000.	5758.670*	0.000	0.	0.	0.00	-0.020	1	0 12:44:16
9000.	5762.893*	0.053	1.	2.	3.00	-0.020	60	0 12:44:33
9000.	5762.891*	0.045	2.	3.	3.00	-0.020	60	0 12:45:58

Traverse 2

SCINTREX V5.2 AUTOGRAV / Field Mode R5.21

Ser No: 711415.

Line: 3. Grid: 0. Job: 1. Date: 06/05/20 Operator: 1.

GREF.:	0. mGals	Tilt x sensit.:	268.6
GCAL.1:	6187.411	Tilt y sensit.:	261.8
GCAL.2:	0.0	Deg.Latitude:	32.67
TEMPCO.:	-0.1260 mGal/mK	Deg.Longitude:	115.5
Drift const.:	1.77	GMT Difference:	7.hr
Drift Correction Start	Time: 15:35:33	Cal.after x samples:	999
	Date: 06/03/02	On-Line Tilt Corrected = "*"	

Station	Grav.	SD.	Tilt x	Tilt y	Temp.	E.T.C.	Dur	# Rej	Time
22.	5763.626*	0.079	1.	12.	3.00	0.014	60	0	09:17:10
30.	5763.616*	0.100	6.	-1.	3.00	0.013	60	0	09:26:19
9000.	5763.588*	0.047	1.	-7.	3.00	0.015	60	0	09:11:06
9000.	5763.565*	0.049	-4.	-7.	3.00	0.012	60	0	09:31:40

SCINTREX V5.2 AUTOGRAV / Field Mode R5.21

Ser No: 711415.

Line: 3. Grid: 0. Job: 1. Date: 06/05/20 Operator: 1.

GREF.:	0. mGals	Tilt x sensit.:	268.6
GCAL.1:	6187.411	Tilt y sensit.:	261.8
GCAL.2:	0.0	Deg.Latitude:	32.67
TEMPCO.:	-0.1260 mGal/mK	Deg.Longitude:	115.5
Drift const.:	1.77	GMT Difference:	7.hr
Drift Correction Start	Time: 15:35:33	Cal.after x samples:	999
	Date: 06/03/02	On-Line Tilt Corrected = "*"	

Station	Grav.	SD.	Tilt x	Tilt y	Temp.	E.T.C.	Dur	# Rej	Time
2104.	5763.761*	0.091	1.	10.	3.00	0.017	60	0	07:46:58
2106.	5763.752*	0.064	-3.	5.	3.00	0.017	60	0	07:50:18
2108.	5763.733*	0.093	1.	5.	3.00	0.018	60	0	07:54:33
2110.	5763.719*	0.076	-3.	4.	3.00	0.018	60	1	07:57:11
2112.	5763.713*	0.079	-2.	5.	3.00	0.018	60	0	08:10:12
2114.	5763.714*	0.075	-5.	4.	3.00	0.018	60	0	08:14:48
2116.	5763.695*	0.107	1.	-0.	3.00	0.018	60	0	08:22:13
2118.	5763.697*	0.080	-1.	6.	3.00	0.018	60	0	08:25:57
2120.	5763.694*	0.072	4.	5.	3.00	0.018	60	0	08:29:46
2122.	5763.684*	0.086	-5.	6.	3.00	0.018	60	0	08:34:00
9000.	5763.698*	0.038	-3.	-0.	3.00	0.017	60	0	07:42:13
9000.	5763.571*	0.039	-5.	-3.	3.00	0.012	60	0	09:33:22

SCINTREX V5.2 AUTOGRAV / Field Mode R5.21

Ser No: 711415.

Line: 3. Grid: 0. Job: 1. Date: 06/05/20 Operator: 1.

GREF.:	0. mGals	Tilt x sensit.:	268.6
GCAL.1:	6187.411	Tilt y sensit.:	261.8
GCAL.2:	0.0	Deg.Latitude:	32.67
TEMPCO.:	-0.1260 mGal/mK	Deg.Longitude:	115.5
Drift const.:	1.77	GMT Difference:	7.hr
Drift Correction Start	Time: 15:35:33	Cal.after x samples:	999
	Date: 06/03/02	On-Line Tilt Corrected = "*"	

Station	Grav.	SD.	Tilt x	Tilt y	Temp.	E.T.C.	Dur	# Rej	Time
122.	5763.096*	0.081	-1.	-1.	3.00	0.078	60	0	20:23:10
124.	5763.098*	0.057	6.	-0.	3.00	0.077	60	2	20:28:08
126.	5763.093*	0.083	2.	-0.	3.00	0.075	60	0	20:33:22
128.	5763.107*	0.076	2.	1.	3.00	0.074	60	0	20:38:27
130.	5763.086*	0.046	3.	-1.	3.00	0.073	60	0	20:42:23
132.	5763.066*	0.056	2.	-3.	3.00	0.072	60	1	20:46:18
134.	5763.079*	0.090	1.	1.	3.00	0.070	60	0	20:51:49
136.	5763.073*	0.073	1.	-1.	3.00	0.068	60	0	21:00:10
138.	5763.062*	0.079	-0.	2.	3.00	0.067	60	0	21:03:32
140.	5763.051*	0.094	2.	1.	3.00	0.065	60	0	21:08:11

142.	5763.057*	0.082	2.	0.	3.00	0.064	60	0	21:12:06
144.	5763.058*	0.086	0.	-0.	3.00	0.063	60	0	21:15:21
146.	5763.063*	0.084	1.	-0.	3.00	0.061	60	0	21:18:10
148.	5763.055*	0.078	0.	1.	3.00	0.060	60	1	21:21:16
150.	5763.056*	0.056	2.	-1.	3.00	0.059	60	0	21:24:41
152.	5763.054*	0.077	2.	-2.	3.00	0.057	60	0	21:27:36
154.	5763.046*	0.083	2.	-2.	3.00	0.055	60	0	21:32:56
156.	5763.043*	0.084	4.	-0.	3.00	0.054	60	0	21:36:24
158.	5763.039*	0.076	1.	-1.	3.00	0.052	60	0	21:39:34
160.	5763.037*	0.098	1.	-2.	3.00	0.049	60	0	21:45:44
162.	5763.028*	0.078	2.	1.	3.00	0.046	60	0	21:52:33
164.	5763.016*	0.062	-0.	-0.	3.00	0.045	60	1	21:55:41
166.	5763.027*	0.078	-1.	2.	3.00	0.043	60	0	21:58:52
168.	5763.024*	0.097	2.	2.	3.00	0.040	60	0	22:03:49
170.	5763.019*	0.077	2.	-1.	3.00	0.038	60	0	22:09:13
172.	5763.014*	0.082	2.	-1.	3.00	0.036	60	0	22:12:53
174.	5763.010*	0.089	1.	-0.	3.00	0.034	60	0	22:16:36
176.	5763.005*	0.094	2.	2.	3.00	0.030	60	0	22:24:00
178.	5762.994*	0.083	1.	-2.	3.00	0.027	60	0	22:29:13
180.	5762.994*	0.048	4.	0.	3.00	0.025	60	0	22:32:37
182.	5762.998*	0.055	2.	2.	3.00	0.023	60	0	22:35:48
184.	5762.985*	0.041	2.	-1.	3.00	0.021	60	0	22:38:59
186.	5762.996*	0.034	-1.	3.	3.00	0.020	60	0	22:42:02
188.	5762.992*	0.036	1.	2.	3.00	0.018	60	0	22:45:09
190.	5762.977*	0.032	-0.	1.	3.00	0.015	60	0	22:48:28
192.	5762.984*	0.049	-0.	3.	3.00	0.014	60	0	22:51:37
9000.	5763.077*	0.054	-0.	-2.	3.00	0.082	60	0	19:29:50
9000.	5762.926*	0.038	5.	-2.	3.00	0.010	60	0	22:57:29

Traverse 3

SCINTREX V5.2 AUTOGRAV / Field Mode R5.21

Ser No: 711415.

Line: 3. Grid: 0. Job: 1. Date: 06/05/20 Operator: 1.

GREF.:	0. mGals	Tilt x sensit.:	268.6
GCAL.1:	6187.411	Tilt y sensit.:	261.8
GCAL.2:	0.0	Deg.Latitude:	32.67
TEMPCO.:	-0.1260 mGal/mK	Deg.Longitude:	115.5
Drift const.:	1.77	GMT Difference:	7.hr
Drift Correction Start	Time: 15:35:33	Cal.after x samples:	999
	Date: 06/03/02	On-Line Tilt Corrected = "*"	

Station	Grav.	SD.	Tilt x	Tilt y	Temp.	E.T.C.	Dur	# Rej	Time
72.	5763.008*	0.045	-1.	-1.	3.00	0.007	60	0	23:02:34
74.	5762.999*	0.053	-0.	1.	3.00	0.005	60	0	23:05:54
76.	5762.996*	0.043	1.	-0.	3.00	0.003	60	0	23:09:43
78.	5762.991*	0.041	4.	2.	3.00	0.001	60	0	23:13:10
80.	5762.984*	0.031	-2.	-0.	3.00	-0.002	60	0	23:17:33
82.	5762.980*	0.047	-1.	-2.	3.00	-0.003	60	0	23:20:09
84.	5762.978*	0.049	-0.	-2.	3.00	-0.005	60	0	23:22:54
86.	5762.976*	0.035	1.	-1.	3.00	-0.007	60	0	23:25:42
88.	5762.975*	0.036	1.	-3.	3.00	-0.008	60	0	23:28:25
90.	5762.962*	0.057	-1.	-2.	3.00	-0.010	60	0	23:31:37
92.	5762.974*	0.045	2.	-1.	3.00	-0.012	60	0	23:34:32
94.	5762.981*	0.042	2.	3.	3.00	-0.013	60	0	23:37:03
96.	5762.971*	0.040	2.	-1.	3.00	-0.015	60	0	23:39:44
98.	5762.972*	0.051	-2.	-1.	3.00	-0.016	60	0	23:42:24
100.	5762.979*	0.048	-1.	1.	3.00	-0.018	60	0	23:44:56
102.	5762.976*	0.047	1.	2.	3.00	-0.019	60	0	23:47:32
104.	5762.971*	0.040	1.	3.	3.00	-0.021	60	0	23:50:17
106.	5762.955*	0.041	2.	0.	3.00	-0.022	60	0	23:52:55
108.	5762.958*	0.044	0.	1.	3.00	-0.024	60	0	23:55:31
110.	5762.965*	0.053	-1.	-0.	3.00	-0.025	60	0	23:57:58
9000.	5763.077*	0.054	-0.	-2.	3.00	0.082	60	0	19:29:50
9000.	5762.898*	0.039	2.	1.	3.00	-0.029	60	0	24:59:38

Traverse 4

SCINTREX V5.2 AUTOGRAV / Field Mode R5.21

Ser No: 711415.

Line: 3. Grid: 0. Job: 1. Date: 06/05/21 Operator: 1.

GREF.:	0. mGals	Tilt x sensit.:	268.6
GCAL.1:	6187.411	Tilt y sensit.:	261.8
GCAL.2:	0.0	Deg.Latitude:	32.67
TEMPCO.:	-0.1260 mGal/mK	Deg.Longitude:	115.5
Drift const.:	1.77	GMT Difference:	7.hr
Drift Correction Start	Time: 15:35:33	Cal.after x samples:	999
	Date: 06/03/02	On-Line Tilt Corrected = "*"	

Station	Grav.	SD.	Tilt x	Tilt y	Temp.	E.T.C.	Dur	# Rej	Time
30.	5762.436*	0.079	2.	10.	3.00	0.049	60	2	10:12:19
32.	5762.400*	0.084	-3.	2.	3.00	0.047	60	0	10:21:23
34.	5762.405*	0.057	-1.	1.	3.00	0.046	60	0	10:24:03
36.	5762.384*	0.074	-2.	-2.	3.00	0.046	60	0	10:26:51
38.	5762.400*	0.069	-1.	4.	3.00	0.045	60	0	10:29:42
40.	5762.385*	0.069	2.	-3.	3.00	0.044	60	0	10:32:42
42.	5762.394*	0.086	-2.	-1.	3.00	0.043	60	0	10:35:24
44.	5762.393*	0.094	-2.	-0.	3.00	0.042	60	0	10:37:56
46.	5762.377*	0.064	-1.	-7.	3.00	0.041	60	0	10:41:30
48.	5762.380*	0.059	-0.	4.	3.00	0.040	60	0	10:44:45
50.	5762.371*	0.091	-4.	0.	3.00	0.039	60	0	10:47:44
52.	5762.366*	0.080	0.	-0.	3.00	0.037	60	0	10:52:42
54.	5762.354*	0.087	3.	-4.	3.00	0.035	60	0	10:57:38
56.	5762.364*	0.079	-4.	-1.	3.00	0.034	60	0	11:00:21
148.	5762.374*	0.083	0.	-6.	3.00	0.027	60	0	11:18:45
150.	5762.380*	0.096	-0.	1.	3.00	0.026	60	0	11:21:49
152.	5762.369*	0.066	-5.	-1.	3.00	0.024	60	0	11:24:37
154.	5762.373*	0.079	-2.	6.	3.00	0.024	60	0	11:27:15
156.	5762.359*	0.084	-2.	10.	3.00	0.023	60	0	11:29:53
158.	5762.373*	0.096	-6.	6.	3.00	0.021	60	0	11:33:01
160.	5762.346*	0.053	-2.	-4.	3.00	0.020	60	2	11:35:41
162.	5762.347*	0.074	-7.	-5.	3.00	0.019	60	0	11:38:24
164.	5762.322*	0.092	-3.	-1.	3.00	0.018	60	1	11:41:15
166.	5762.340*	0.078	-5.	-5.	3.00	0.017	60	0	11:43:53
168.	5762.348*	0.088	-8.	-1.	3.00	0.016	60	0	11:46:56
170.	5762.331*	0.061	-2.	0.	3.00	0.013	60	0	11:53:06
172.	5762.331*	0.072	1.	2.	3.00	0.012	60	0	11:55:54
174.	5762.324*	0.061	-0.	-1.	3.00	0.010	60	0	12:00:30
176.	5762.326*	0.077	-1.	0.	3.00	0.009	60	0	12:03:54
178.	5762.323*	0.059	1.	3.	3.00	0.007	60	0	12:08:18
180.	5762.312*	0.064	-2.	-0.	3.00	0.005	60	0	12:13:11
182.	5762.313*	0.075	-1.	-1.	3.00	0.003	60	0	12:18:43
184.	5762.292*	0.065	-0.	-1.	3.00	0.002	60	1	12:22:11
188.	5762.294*	0.079	-1.	-3.	3.00	0.000	60	0	12:25:12
190.	5762.295*	0.092	-2.	1.	3.00	-0.001	60	0	12:27:44
192.	5762.286*	0.078	-1.	-7.	3.00	-0.002	60	0	12:31:24
194.	5762.301*	0.095	-2.	-4.	3.00	-0.004	60	0	12:36:56
196.	5762.284*	0.072	-5.	-1.	3.00	-0.005	60	0	12:39:19
198.	5762.286*	0.087	3.	1.	3.00	-0.006	60	0	12:41:35
200.	5762.278*	0.091	0.	-3.	3.00	-0.007	60	0	12:43:48
202.	5762.263*	0.075	-2.	-6.	3.00	-0.009	60	0	12:48:02
204.	5762.263*	0.087	4.	-1.	3.00	-0.010	60	0	12:50:28
9000.	5762.346*	0.052	-0.	0.	3.00	0.051	60	0	10:06:15
9000.	5762.191*	0.051	-3.	3.	3.00	-0.012	60	0	12:59:14

Appendix G – Clandestine Tunnels Data Points

Traverse 1

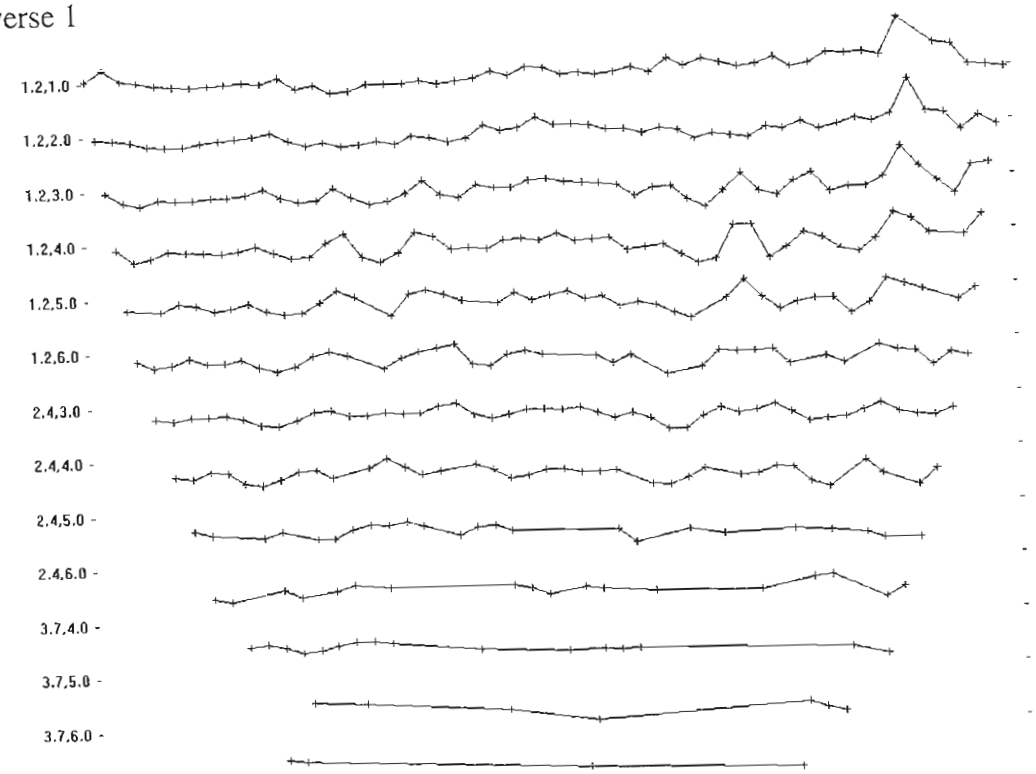

Traverse 2

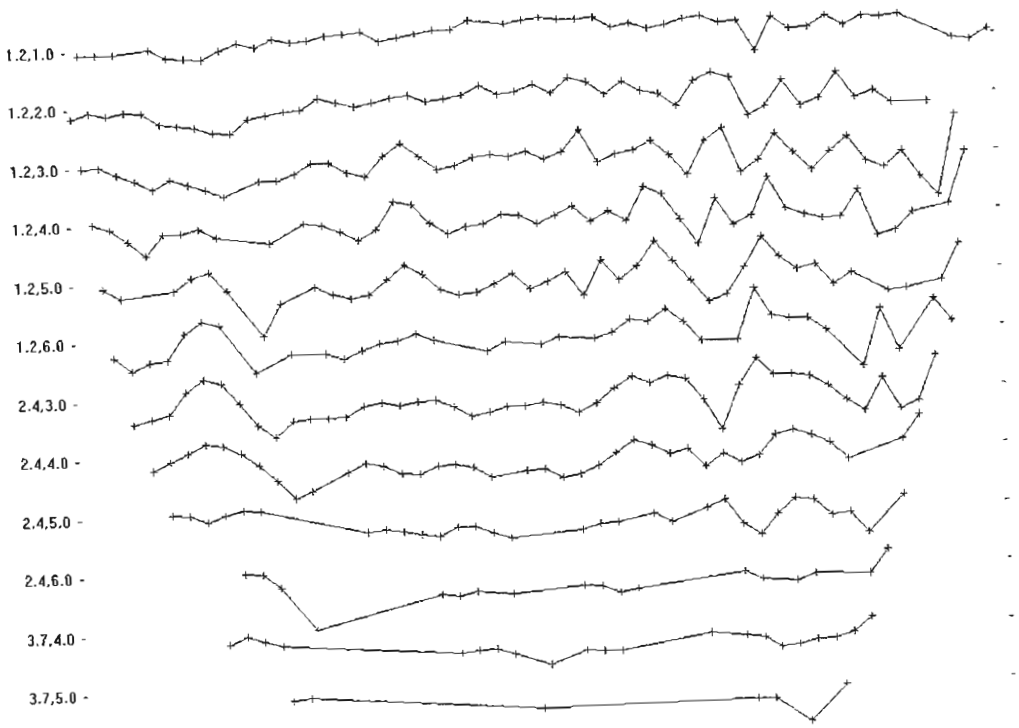

Traverse 3

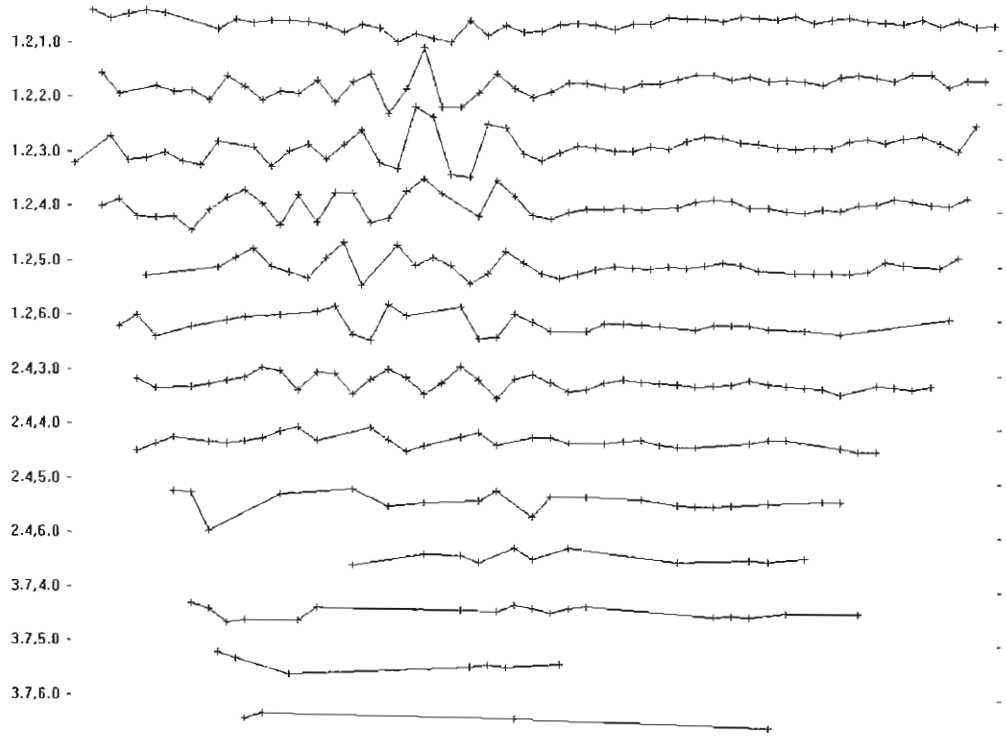

Traverse 4

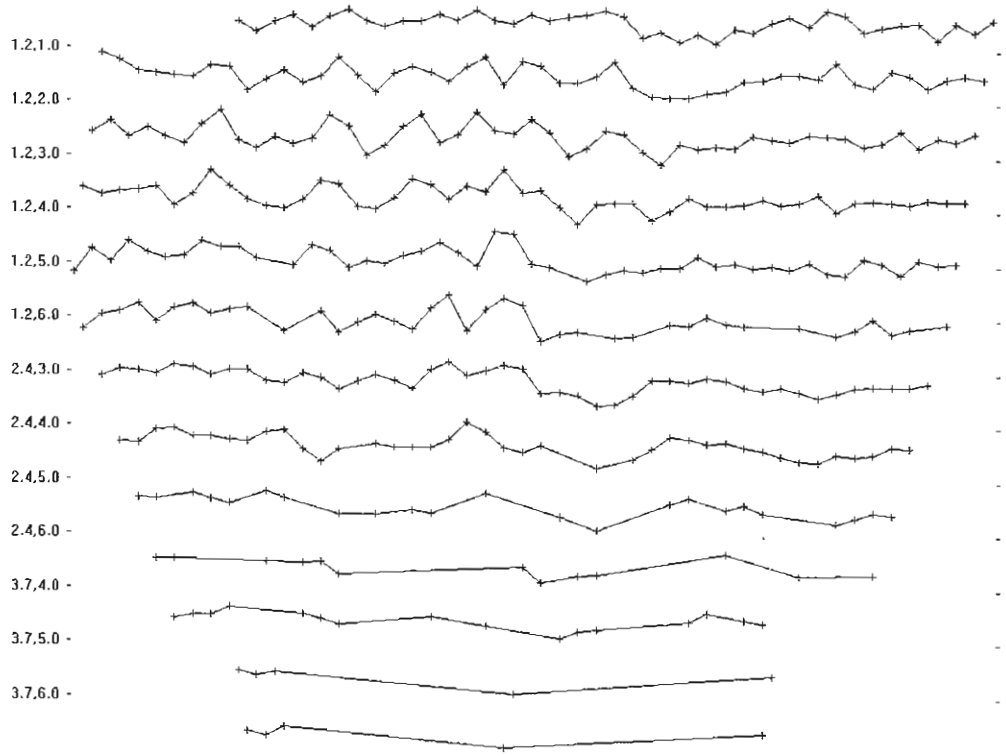

Traverse 5

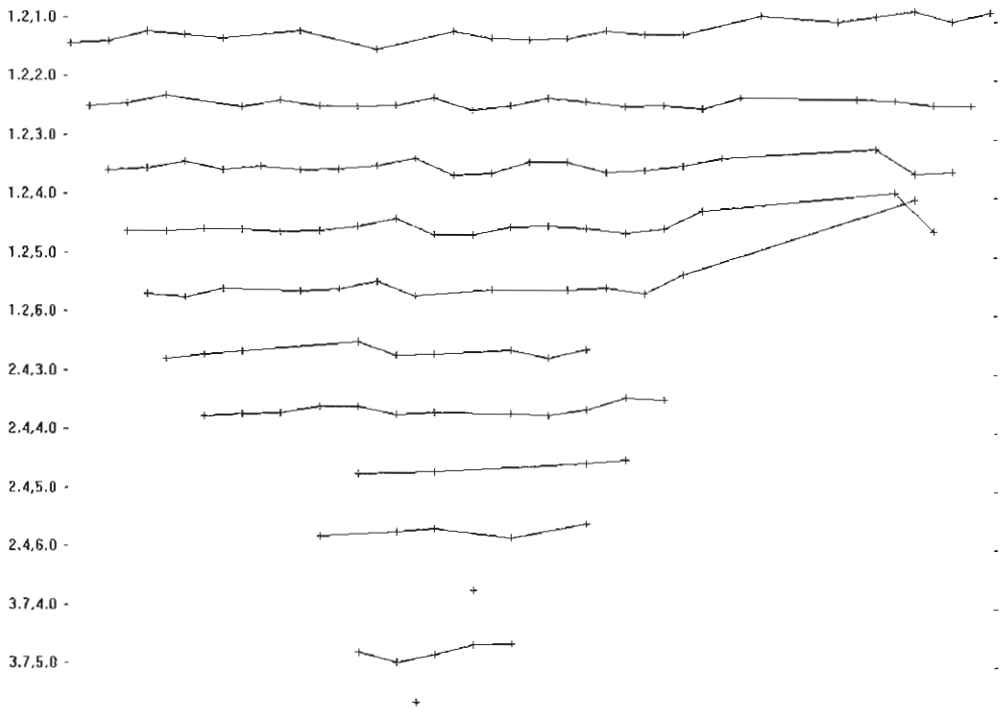

BIBLIOGRAPHY

Advanced Geosciences, Inc. (2006) Retrieved August 15, 2006, web site: http://www.agiusa.com/supersting-r1.shtml

Blanchard, C.M. (2005) Al Qaeda: Statements and evolving ideology. Congressional Research Service – Report for Congress (RL32759). Washington, D.C.: 4-10.

Danielson, K. (2000) Geology of the south snake range. National Park Service, 1-2.

Fraiser, T. (2006) Phone Interview. February, 2006.

Garland, G.D. (1965) Gravity anomalies and structures in the Earth's crust, in The Earth's shape and gravity. Pergamon Press Ltd., New York, N.Y.: 101-127.

Gilmore, T.D. and R.O. Castle (1983) Tectonic preservation of the divide between the Salton basin and the Gulf of California. *Geology*, 11, 474-477.

Google Earth (2005) Europa Technologies
Software: Image © 2006 NASA and TerraMetrics
Accessed: 4September2006

Grabowski Jr., G.J. (1985) Mississippian system, in R.C. McDowell (ed.) The Geology of Kentucky- A Test to Accompany the Geologic Map of Kentucky. U.S. Geological Survey Professional Paper 1151-H, Technical Report: H 19-31.

Grant, F.S. and G.F. West (1965) Introduction to the gravity and magnetic method, in Interpretation theory in applied geophysics. McGraw-Hill Book Company, New York, N.Y.: 189-209.

International Boundary Water Commission (2008) Retrieved July 22, 2008, web site: http://www.ibwc.state.gov/

Jakosky, J.J. and R.H. Hopper (1937) The effect of moisture on the direct current resistivities of oil sands and rocks. *Geophysics*, 2(1), 33-54.

Kramer, S.R., McDonald, W.J. and J.C. Thomson (1992) Background, in An introduction to trenchless technology. Van Nostrand Reinhold, New York, N.Y.: 17-35.

Kramer, S.R., McDonald, W.J. and J.C. Thomson (1992) Creating the hole, in An introduction to trenchless technology. Van Nostrand Reinhold, New York, N.Y.: 36-66.

Kramer, S.R., McDonald, W.J. and J.C. Thomson (1992) Pipe jacking and microtunnelling, in An introduction to trenchless technology. Van Nostrand Reinhold, New York, N.Y.: 86-120.

Lillie, R.J. (1999) Whole Earth geophysics: An introductory textbook for geologists & geophysicists. Chapter 8 gravity and isostasy. Prentice Hall, Upper Saddle River, N.J.: 223-283.

Loke, M.H. (1998) RES2DINV ver. 3.3 for windows 3.1, 95, and NT: Rapid 2D resistivity and IP inversion using the least-squares method Wenner, dipole-dipole, inline pole-pole, pole-dipole, equatorial dipole-dipole, Schlumberger on land, underwater and cross-borehole surveys. Penang, Malaysia, 1-66.

Lowry, T. and P.N. Shive (1990) An evaluation of Bristow's method for the detection of subsurface cavaties. *Geophysics*, 55(5), 514-520.

Marks, J.B. (1950) Vegetation and soil relations in the lower Colorado Desert. *Ecology*, 31(2), 176-193.

McDowell, R.C. (1985) Structural geology, in R.C. McDowell (ed.) The Geology of Kentucky- A Test to Accompany the Geologic Map of Kentucky. U.S. Geological Survey Professional Paper 1151-H, Technical Report: H 53-59.

Medalia, J. (2005) Nuclear terrorism: A brief review of threats and responses. Congressional Research Service – Report for Congress (RL 32595). Washington, D.C.: 1-4.

Micro-g LaCaste (2006) Retrieved August 8, 2006, web site: http://www.microgsolutions.com/

Miró, R.J. (2003) Organized crime and terrorist activity in Mexico, 1999-2002. Federal Research Division – Library of Congress, Washington, D.C.: 1-49.

Morrison, R.B. (e.d.) (1991) Quaternary nonglacial geology: Conterminous U.S. Chapter 11 quaternary geology of the Basin and Range Province in California. *The Geology of North America, Inc.*, Boulder, CO: k-2, 321-352.

Morton, P.K. (1977) Geology, in Geology and Mineral Resources of Imperial County, California. County Report 7, California Division of Mines and Geology, Sacramento, C.A.: 13-24.

Newell, W.L. (1985) Physiography, in R.C. McDowell (ed.) The Geology of Kentucky- A Test to Accompany the Geologic Map of Kentucky. U.S. Geological Survey Professional Paper 1151-H, Technical Report: H 65-68.

Picha, J. (1973) Introduction, in Pick, M., Picha, J. and V. Vyskočil Theory of the Earth's Gravity Field. Elsevier Scientific Publishing Company, Czechoslovakia: 15-18.

Reheis, M.C. (2005) Geologic and biotic perspectives on ate Cenozoic drainage history

of the southwestern Great Basin and lower Colorado River region: Conference Abstract. U.S. Department of the Interior, USGS: Desert Studies Center, Zzyzx, C.A.: 1-19.

Schonfeld, R.G. (1969) The early development of California's Imperial Valley. *The Historical Society of Southern California*, San Diego, C.A.: 284-422.

Seigel, H.O. (1995) A guide to high precision land gravimeter surveys. Scintrex Limited, Ontario, Canada: 1-115.

Sheriff, R.E. (2002) Encyclopedic dictionary of applied geophysics. 13th geophysical references series, *Society of Exploration Geophysicists*, 4th Edition, Tulsa, OK: 1-402.

Sterling, R.L., Friant, J.E., Garbesi, V.A., Meinholz, J.H. and T.D. O'Rourke (1989) Micro- and small-diameter tunneling. *National Academy Press.*, Washington, D.C. 3-22.

Taminskas, J., Paskauskas, R., Zvikas, A., and J. Satkunas (2006) Karst and ecosystems, in I.S. Zektser (ed.) Geology and Ecosystems. International Union of Geological Sciences (IUGS), Springer-Science+Business Media, Inc., New York, N.Y.: 61-76.

Telford, W.M., Geldart, L.P. and R.E. Sheriff (1990) Applied geophysics. 2. Gravity methods. Cambridge University Press. 2nd Edition, New York, N.Y.: 6-61.

Telford, W.M., Geldart, L.P., Sheriff, R.E. and D.A. Keys (1976) Gravity methods, in Applied geophysics. Cambridge Unversity Press. New York, N.Y.: 7-104.

Thorne, R.F. (1986) A historical sketch of the vegetation of the Mojave and Colorado deserts of the American southwest. *Ann. Missouri Bot. Guard.*, 73, 642-51.

United States. Department of Energy (2004) Affected environment, in Final Environmental Impact Statement for the Imperial-Mexicali 230-kV transmission lines. Department of the Interior (DOE/EIS-0365). El Centro, CA: (1), 1-99.

United States. Department of Energy (2006) Terrorist Countries List. Retrieved August 23, 2006, web site: http://www.ch.doe.gov/offices/OCI/TerroristCountries/

United States. Department of Homeland Security (2004) Review of the status of Department of Homeland Security efforts to address its major management challenges. Office of Inspector General (OIG-04-21). Washington, D.C.: 26-43.

United States. Department of Homeland Security (2005) Fact Sheet: Secure Border Initiative. Retrieved December 10, 2005, web site: http://www.dhs.gov/dhspublic/interapp/press_release/press_release_0794.xml

Waters, M.R. (1983) Late Holocene lacustrine chronology and archeology of ancient Lake Cahuilla, California. *Quaternary Research*, 19, 373-87.

Zimmerman, R.P. (1981) Tables, in Soil Survey of Imperial County California Imperial Valley Area. United States Department of Agriculture Soil Conservation Service: (n.l.) 80-105.